Norges miljø- og
biovitenskapelige
universitet

Master`s Thesis 2019 30 ECTS

Faculty of Environmental Sciences and Natural Resource Management
(MINA)

Wind Power Forecasting

Physical Modelling

Alexander Dybvad
Renewable Energy

Acknowledgments

I would like to express my gratitude to the people who have supported me during this process of writing my thesis. Firstly, I would like to thank my supervisor Arne Gravdahl at WindSim AS for taking the time and energy to guide me through this process. Additionally, I wish to thank the team at WindSim AS for opening their office and contributing with some much-needed guidance. Furthermore, a big thank to Thea von Hirsch and Håkon Kjersem for sparring with me during the last year, together with my classmates, you made the time at NMBU great. A special thanks to my family and friends for their support. And finally, thanks to Ole Gunder Skiaker for always being at the other end of the rope and of course Hanne Sofie Hammer for her patience and love.

Ås, Norway

15.05.2019

Abstract

With the stochastic nature of wind power and the increased penetration of wind power in the energy system, new challenges become eminent. For the Transmission System Operators (TSOs), the increased penetration of wind power in the energy system makes the task of balancing the energy system more demanding. With the challenge of recreating actual wind conditions at the wind farms, physical modelling is becoming a preferred method. It has proven to increase the accuracy in wind power predictions. The use of computational fluid dynamics (CFD) has shown to be especially beneficial in complex terrain. To reduce the uncertainties in the wind power predictions, this thesis seeks to analyse the benefits of using CFD in wind power forecasting. With the work of analysing the potential benefits, two forecasting methods are tested. The first method uses an equivalent power curve and forecasted wind speed data from the weather service provider Yr. The second method combines the CFD program WindSim together with the forecasted wind speed data from Yr. The two forecasting methods are tested at the following wind farm locations in Norway: Bessakerfjellet, Hitra, Smøla, Valsneset and Ytre Vikna. The physical and CFD method performed the best in three out of the five cases analysed. In the case of Bessakerfjellet, Hitra and Valsneset, the use of CFD produced forecast with prediction errors of 16.56%, 16.64%, 15.58%, measured in normalized mean absolute error (NMAE). At Smøla and Ytre Vikna, the equivalent power curve obtained a prediction error of 13.21%, 20.69%. The findings indicate that the use of CFD and WindSim can contribute to more accurate wind power prediction.

Sammendrag

Med vindens stokastiske natur og den økte andelen av vindkraft i energisystemet, medfører dette nye utfordringer. For Statnett som transmisjonssystemoperatør (TSO), medfører den økte andelen av vindkraft at oppgaven med å balansere energisystemet blir mer krevende. Det å gjenskape og estimere faktiske vindforhold i en vindpark er en utfordrende oppgave. Fysisk modellering eller numerisk modellering (CFD) er blitt en av de foretrukne metodene for å kunne beskrive vindens bevegelse. CFD har også vist seg å kunne bidra til økt presisjon, og i vindparker med komplekst terreng har resultatene vist seg å være spesielt gode. For å redusere usikkerhetene i vindkraftforutsetningene, søker denne oppgaven å analysere fordelene ved å bruke CFD i vindkraftprognoser. For å kunne analysere de potensielle fordelene, testes to prognosemetoder. Den første metoden bruker turbinens ekvivalente effektkurve sammen med vindhastighetsdata fra værvarslingstjenesten Yr. Den andre metoden kombinerer CFD-programmet WindSim med værvarslet fra Yr. De to prognosemetodene har blitt testet på følgende vindparker i Norge: Bessakerfjellet, Hitra, Smøla, Valsneset og Ytre Vikna. CFD- baserte metoden gjorde det best i tre av de fem analyserte vindparkene. For Bessakerfjellet, Hitra og Valsneset produserte CFD-metoden produksjonsestimater med en prediksjonsfeil på henholdsvis 16,56%, 16,64%, 15,58%, målt i normalisert gjennomsnittlig absolutt feil (NMAE). Ved Smøla og Ytre Vikna oppnådde metoden basert på turbinens ekvivalente produksjonskurve en prediksjonsfeil på henholdsvis 13,21%, 20,69%. Funnene fra analysene tyder på at kombinasjonen av CFD og WindSim kan bidra positivt til mer presise produksjonsestimater.

Table of Contents

Acknowledgments ..... *ii*

Abstract ..... *iv*

Sammendrag ..... *vi*

1 Introduction *1*

1.1 Motivation **1**

1.2 Goal, Scope and Limitations **2**

1.3 Background **2**

1.4 Structure and Layout **3**

2 Theoretical Background *4*

2.1 The Wind Resource **4**

2.1.1 Introduction 4

2.1.2 Temporal and Spatial Characteristics of Wind 5

2.1.3 Wind and the Characteristic of the Atmospheric Boundary Layer 7

2.1.4 Determining the Wind Profile 7

2.1.5 Surface Roughness and Terrain Classifications 7

2.1.6 Available Power and Potential Energy 8

2.2 Harvesting the Kinetic Energy **9**

2.2.1 Wind Turbines and Wind Farms 9

2.2.2 The Power Curve 10

2.3 Transmission System Operator **11**

2.4 Wind Power Forecasting **12**

2.4.1 Wind Power Forecast Time Scales 12

2.4.2 Forecast Methods 13

2.4.3 Rapid Changes in The Wind 14

2.5 Modelling the Physical World **15**

2.5.1 The Foundation of CFD 15

2.5.2 Finite Volume Method 16

2.5.3 Infinitesimal Fluid Element 16

2.5.4 Navier - Stokes Equations 17

2.6 WindSim **17**

2.6.1 The Approach 18

3 Models, Data and Methodology 19

3.1 The Wind Farms 19

3.2 Data Foundation 20

3.2.1 Norwegian Metrological Institute and Yr.no 20

3.2.2 Norwegian Water Resource and Energy Directorate 21

3.2.3 Synchronizing the Datasets 22

3.3 The Forecasting Methods 23

3.4 Linear Interpolation of The Power Curve 24

3.5 Windographer 25

3.6 Designing the Wind Farms in WindSim 25

3.6.1 Terrain 25

3.6.2 Wind Fields 27

3.6.3 Objects 27

3.6.4 Energy 29

3.7 Benchmarking and Uncertainty Analysis 29

4 Results 30

4.1 Bessakerfjellet 30

4.1.1 Overall Production Forecast 30

4.1.2 Forecast Error 31

4.2 Hitra 32

4.2.1 Overall Production Forecast 32

4.2.2 Forecast Error 33

4.3 Smøla 34

4.3.1 Overall Production Forecast 34

4.3.2 Forecast Error 35

4.4 Valsneset 36

4.4.1 Overall Production Forecast 36

4.4.2 Forecast Error 37

4.5 Ytre Vikna 38

4.5.1 Overall Production Forecast 38

4.5.2 Forecast Error 39

4.6 Overall Results 40
4.7 Calibration Point Height Analysis 41
4.8 Periods of Interest 42
4.8.1 Production and Prediction Inconsistency 42
4.8.2 Ramp Events 43
4.8.3 Period with High Accuracy 44
5 Discussion 45
5.1 The Data Foundation 45
5.1.1 Time Scales 45
5.2 Developing the WindSim Models 46
5.2.1 Grid Resolution and Computer Capacities 46
5.2.2 Wake Modelling 47
5.2.3 Selected Height for the Calibration Point 47
5.3 Theoretical Power Curve 47
5.4 Challenges with Forecasted Wind Speed 48
5.4.1 Ramp Events 48
5.4.2 Timing 48
5.4.3 Production and Forecast Inconsistency 48
6 Conclusion 49
6.1 Conclusion 49
6.2 Future Work 49
7 References 50
8 Appendix A – Wind Turbine Effect Curves 52
9 Appendix B – WindSim Report 54

List of Figures

Figure 1 – Surface winds of the general circulation (Hiester & Pennell, 1981) 4
Figure 2 – Time and spatial scale of the atmospheric motion. (Spera, (1994) in Manwell et al. (2010)) 5
Figure 3 – Seasonal changes in wind speeds (Hiester & Pennell, 1981) 6
Figure 4 – Illustration of log-profile over terrain with different roughness's. Inspired by Wegley et al. (1980) 8
Figure 5 – Schematics of an horizontal axis turbine (US Department of Energy, 2018) 10
Figure 6 – Illustration of a wind turbine power curve 11
Figure 7 - Illustration of ramp up (Left circle) and ramp down (right circle). Inspired by Greaves et al. (2009). 15
Figure 8 – A) The finite volume method. B) Infinitesimal fluid element (Anderson & Wendt, 1995) 16
Figure 9 – Basic Course – WindSim. Real world vs. terrain model (3D) (Gravdahl, 2019) 17
Figure 10 – Location of the wind farms (NVE Atlas, 2019) 19
Figure 11 – Snippet of flagged time steps as "invalid" in Windographer. 22
Figure 12 – Graphical description of the two forecasting methods 23
Figure 13 – Interpolation between wind speed bins 24
Figure 14 – Digital terrain model (left) and refinement area (right) of Ytre Vikna. Turbine placement visualized with triangles 26
Figure 15 – Example of refinement in the vertical z-direction for Smøla wind farm 27
Figure 16 – Wind flow calibration for each turbine 28
Figure 17 – Production forecast Bessakerfjellet 30
Figure 18 – Forecast error Bessakerfjellet 31
Figure 19 – Production forecast Hitra 32
Figure 20 – Forecast error Hitra 33
Figure 21 – Production forecast Smøla 34
Figure 22 – Forecast error Smøla 35
Figure 23 – Production forecast Valsneset 36
Figure 24 – Forecast error Valsneset 37

Figure 25 – Production forecast Ytre Vikna 38
Figure 26 – Forecast error Ytre Vikna 39
Figure 27 – Power + CFD to Wind Forecast Error at Bessakerfjellet 41
Figure 28 – Production and prediction inconsistency 42
Figure 29 - Ramp event Valsneset 43
Figure 30 – Ramp event at Smøla 43
Figure 31 – Rapid change in wind speed at Smøla wind farm 44

List of Tables

Table 1 – Wind power forecast time scale classifications (Zhao et al. (2011) and Wang et al. (2011). 13
Table 2 – The three first entries in the times series for Smøla wind farm 20
Table 3 – The three first entries in the NVE time series 21
Table 4 – Selected wind turbines 29
Table 5 – Overall forecast error for 2017. 40
Table 6 – Calibration height analysis for Bessakerfjellet Wind Farm 41

1 Introduction

1.1 Motivation

On the road towards a society propelled by renewable energy, the search for the most promising renewable energy resources (RES) continues. Leading the race, is wind power which is becoming one of the prominent investment areas. In 2018, the Norwegian Minister of Petroleum and Energy, Terje Søviknes, stated at a wind power conference that the rate of construction was significantly higher than the historical average after adopting the Norwegian Energy Act in 1991. In 2018 there were 3,6 Terawatt hours (TWh) of wind energy in Norway, by 2020 the number is expected to reach 10TWh (Søviknes, 2018). The increased installation of wind energy is not only a Norwegian trend, it is also a global trend. In the Energy Transition Outlook 2018 published by DNV-GL, the global installation of wind energy is expected to reach 5000 TWh by 2030, compared to 833 TWh in 2016 (DNV-GL, 2018).

Traditionally, power production has been dominated by regulatable fossil fuels, typically coal, gas and nuclear power. With the shift towards renewable energy, the act of balancing the energy system becomes a demanding challenge, due to the stochastic nature of the RES. For the Transmission System Operator (TSO), the increased penetration of renewables in the energy system makes the task of balancing the system more demanding. Not knowing has a cost, and accurate wind power forecast could contribute to more efficient energy systems (Foley et al., 2012). Wind power predictions in short, medium and long time horizons are all seen to be beneficial and adds value to the wind power sector.

To obtain more precise forecasts, the implementation of physical modelling is becoming more prominent. Traditionally, statistical methods have been the preferred approach, but with wind farms placed in complex terrain, the influence from the physical aspects seems to have significant influence on the wind field. With the work of investigating this effect, this thesis aims to analyse how the use of computational fluid dynamics (CFD) and forecasted wind speeds could produce precise wind power forecasts.

1.2 Goal, Scope and Limitations

With the motivation of contributing to the implementation of more renewable energy, the main objective is to analyse two different forecasting strategies and determine the most accurate method when combined with forecasted wind speed. The first forecasting method is based on an equivalent wind power curve combined with a forecasted time series containing wind speeds. The second method includes the use of a CFD simulation program called WindSim, together with the same time series used in the first method described.

The project scope is limited to five established Norwegian wind farms and the two forecasting methods are applied in each site. Even though, a larger time series would have been preferable, the project is limited to analysing a time series for one year. CFD simulation models require strong computational resources to run models in high resolution. This project has been developed on a standard laptop, which have restricted the resolution of the models.

1.3 Background

With the act of balancing the supply and demand in the power system, the TSO is responsible for balancing the supply and demand in the power system. Previous, the power system has primarily been driven by regulatable thermal-, nuclear- or hydro power. The increased penetration of RES and their stochastic nature makes the work of balancing the system more challenging. More accurate production forecast would decrease the need of additional balancing energy and reserve capacities when integrating more wind energy (Foley et al., 2012). Accurate wind power forecast would also enable the TSO to optimize their dispatch, scheduling and reserve strategies, and contribute to more competitive market trading (Foley et al., 2012).

Wind power forecasting is not a new research field. There are primarily two categories of forecast methods, the statistical and the physical method (Lei et al., 2009). A majority of wind power predictions utilizes statistical method, e.g. auto regressive (AR), moving average (MA), autoregressive moving average (ARMA) and autoregressive integrated moving average (ARIMA), which all seek to analyse historical data and predict future values (Foley et al., 2012). Another statistical method is the use of Artificial Neural Networks (ANN). This method has

provided good results, but one of the limitations is the need of adequate historical data (Li et al., 2013). ANN is often described as a “black box”, due the challenges of not knowing what is physically happening (Corbo et al., 2015). The ANN system learns from their experience, and therefore improves the accuracy when it is developed over time (Foley et al., 2012).

The physical method includes, as the name implies, the physical aspects of nature when estimating wind power predictions. Landberg and Watson (1994) are among the pioneers when it comes to physical modelling. Giebel et al. (2006) also advocated for the use of physical models, especially in complex terrain. In a research study in Alaiz, Spain, they analysed the effects of using advanced physical modelling. By combining inputs from Numerical Weather Prediction (NWP) models with high resolution CFD codes, the findings showcased improvement of error measurements in wind speed and power forecasts, and their conclusion were that the use of CFD could improve the accuracy of the forecast. Corbo et al. (2015) also analysed the benefits of combining statistics and CFD. Their findings supported the positive effects of applying CFD, compared to a single-handed statistical approach. The CFD model also managed to detect local variations recirculation’s, due to the local orography which influenced the performance of the wind farm.

1.4 Structure and Layout

Chapter 1 will present the motivation and aim, together with the scope and limitations of this project. Chapter 2 present the theoretical framework which the projects is based and built upon. In chapter 3 the data foundation is presented together with a description of the methods that have been applied. Chapter 4 will present the results before chapter 5 will discuss the findings. At the end, chapter 6 provide a conclusion to the findings, and highlight some aspects that could be further investigated in future work.

2 Theoretical Background

With the challenge of addressing the subject of this thesis, it is necessary to analyse previous research to understand the complexity of wind forecasting. This chapter will provide insight to the fundamentals of the wind resource, wind power technology, the methods used and how they are applied in wind energy forecasting. Section 2.1 to 2.4 will cover the fundamentals of the wind resource, modern wind power technology and wind power forecasting methods. Section 2.5 will describe the basics of physical modelling and section 2.6 explain the methods in WindSim.

2.1 The Wind Resource

2.1.1 Introduction

As the sun orbits the earth the temperature in the atmosphere fluctuates and causes pressure differences. In a global perspective, the solar radiation strikes equator directly, while at the poles the sun reaches the surface tangential. This variation in radiant energy per unit area causes air to rise at the equator, before it sinks down when the air cools at the southern and northern pole (Hiester & Pennell, 1981). Figure 1 illustrates a simplified description of the wind patterns on a global scale. Fundamentally, there are four atmospheric forces action upon the wind; the Coriolis effect, inertial forces caused by large-scale circular motion and friction caused by earth's surface (Manwell et al., 2010). In more refined scales, the wind`s circulation becomes more intricate and the need for a more detailed description is necessary.

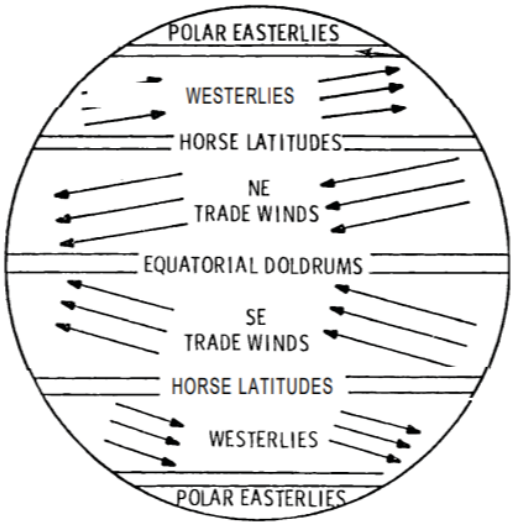

Figure 1 – Surface winds of the general circulation (Hiester & Pennell, 1981)

2.1.2 Temporal and Spatial Characteristics of Wind

Understanding the wind flow is a challenging task, due to the complexity and influence of numerous factors. With the fundamental factors mentioned previously, air pressure, temperature and orographic barriers also becomes important when you want to understand the nature of the wind resource (Manwell et al., 2010).

The characteristics of the wind stretches vastly in both time and the spatial scale. Manwell et al. (2010) provides the following categorizations and descriptions. At the global scale, weather patterns occur over time periods of weeks and months while simultaneously covering large areas. This could e.g. be wind streams like the polar jet streams, which have great influence on the global weather. The synoptic scale stretches over thousands of kilometres and occurs over several days. Weather events at this scale is important when producing long-term weather forecast. Hurricanes and thunderstorms are typical events on the synoptic scale. On the more local scale we have the meso scale. Typical meso scale weather phenomena`s are sea-breeze and mountains winds. These phenomena`s influences areas from tens to hundreds of kilometres and could last up to a day. The smallest scale is the microscale. Orography and air flows passing over regions of higher altitude could create microscale weather phenomena`s such as turbulence and speed ups or having blocking effects. The time and spatial scale of the atmospheric motion can be seen in figure 2.

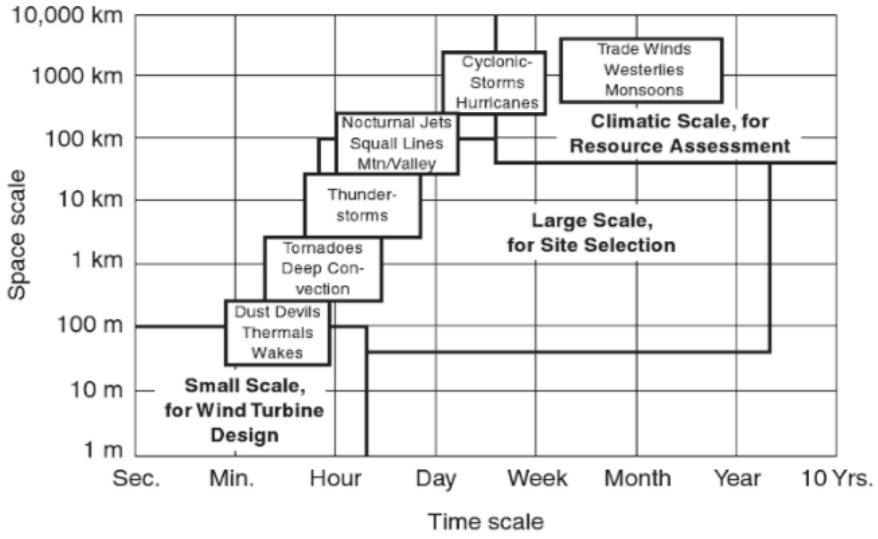

Figure 2 – Time and spatial scale of the atmospheric motion. (Spera, (1994) in Manwell et al. (2010))

Time variations in wind speed is described in four different categories in Hiester and Pennell (1981): *Inter – annual* where the fluctuation in wind speed exceeds a time scale of one year. This category is important for a wind farm developer and the inter-annual variation will be important for Annual Energy Production (AEP) estimates used in resource assessments. *Annual* variations are connected to the seasonal changes that occur during a year. The annual cycle between the four seasons – summer, autumn, winter and spring have significant influence on the wind speeds. The winter months will have the highest average wind speeds. An example of the annual wind speed cycle over a period of three years can be seen in Figure 3.

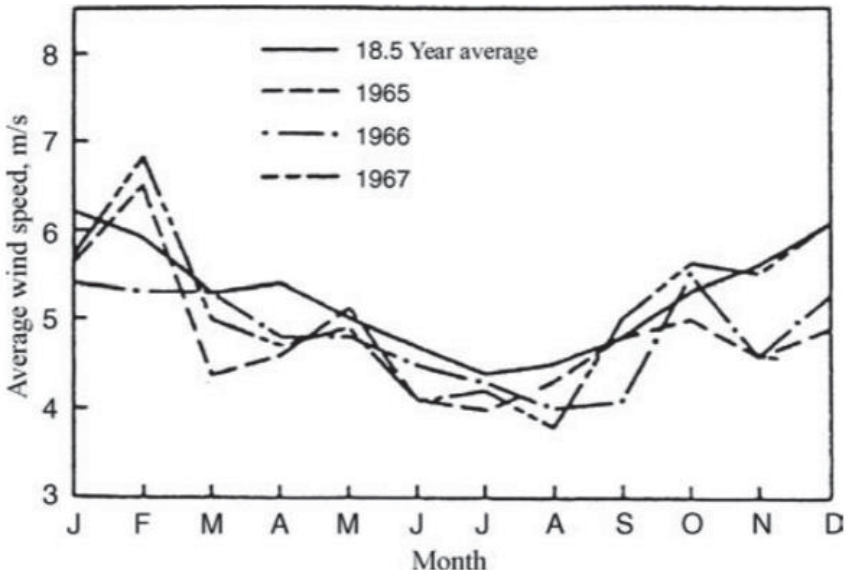

Figure 3 – Seasonal changes in wind speeds (Hiester & Pennell, 1981)

Diurnal variations are the fluctuations of wind speed during a day and is caused by the heating of earth`s surface by solar radiation. There will also be variation caused by geographical location and altitude (Manwell et al., 2010). *Short term* variations, generally over periods less than ten minutes are also of great importance. In short time periods, down to a few seconds, turbulence or non-laminar flow can occur. These random wind speeds fluctuating around the average wind speed could potentially have great influence. It can cause losses in energy production or in worst case, cause damages on the turbine installation (Manwell et al., 2010).

The task of forecasting average wind speeds are complex, and it requires adequate amounts of historical data, preferably over several decades (Manwell et al., 2010). In terms of wind

project development, the resource analysis is commonly based on local wind measurements over a period of few years. Aspliden et al., (1986) supports a statistical established principle implying that one year of climate data can generally be adequate for an approximation of seasonal average winds within an accuracy of 10% and a confidence interval of 90%.

2.1.3 Wind and the Characteristic of the Atmospheric Boundary Layer

Understanding the interaction between terrain features and the wind flow is essential when analysing wind farms. Terrain features could cause velocity variations, wind accelerations and irregular wind shear (Manwell et al., 2010). The atmospheric boundary layer (ABL) is the closest layer to the ground and the characteristics of it are directly influenced by the interaction with the surface of the earth (Manwell et al., 2010) In this domain, the physical quantities e.g. velocity, temperature and humidity can rapidly shift and therefore influence the wind resource (Manwell et al., 2010). With an increased height from the ground, a variation in the wind speed occur. This variation in wind speed is referred to as the vertical wind profile or wind shear, and it is of great importance when analysing wind farm locations (Manwell et al., 2010).

2.1.4 Determining the Wind Profile

There are several methods of describing the vertical wind profile, but one of the classic methods is the logarithmical wind profile. To calculate the wind speed at height z (U_z), equation 1 can be used together with U^* being the friction velocity, k = 0,4 (von Karman`s constant), z_0 the roughness length to estimate the wind speed (Manwell et al., 2010).

Logarithmic profile:
$$U_z = \frac{U^*}{k} ln\left(\frac{z}{z_0}\right) \quad [1]$$

2.1.5 Surface Roughness and Terrain Classifications

Combined with the physical aspects of the ABL, as described in equation 1, changes in the wind profile are caused by alternation in terrain roughness. The effects of wind profiles passing over surfaces with surface roughness varying from high to low can be seen in Figure 4.

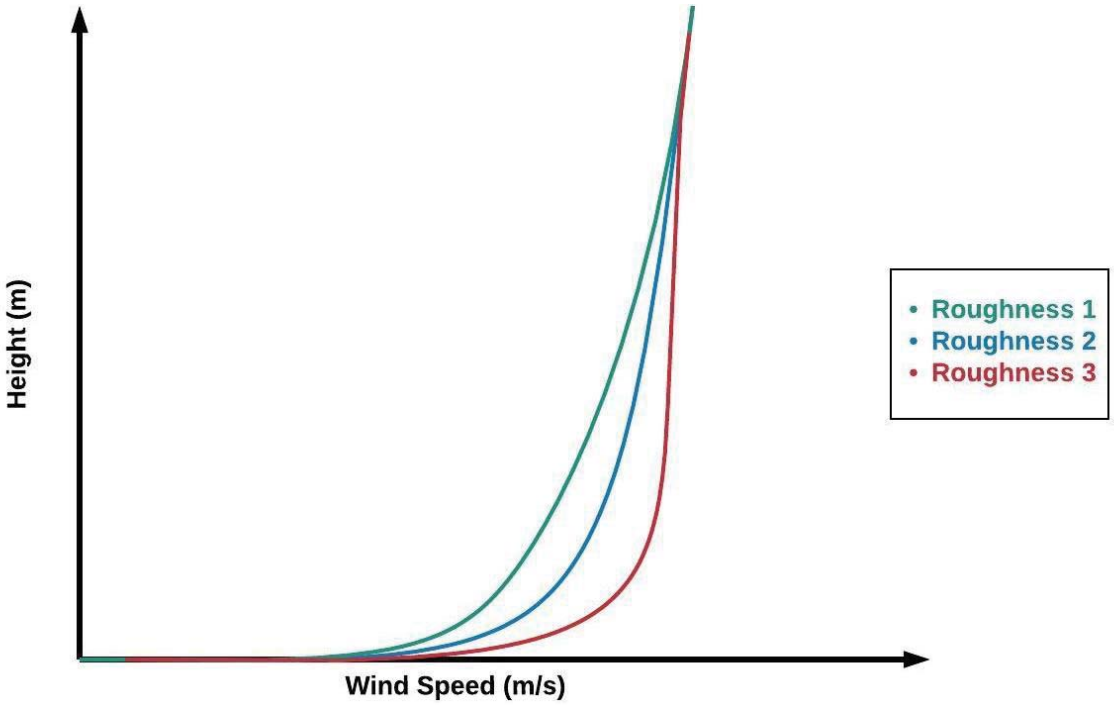

Figure 4 – Illustration of log-profile over terrain with different roughness's. Inspired by Wegley et al. (1980)

The variation in roughness will as the figure illustrates, influence the wind profile. Small forests and grasslands reduce the wind profile in the summertime, but in the winter when the area is covered in snow, the friction from the surface will have different attributes. The effect from the terrain is thoroughly discussed in the literature. Hiester and Pennell (1981) and Wegley et al. (1980) have both proposed different methods of classifying the terrain and its effect on the wind characteristics. The simplest classification is: flat and non-flat terrain. Flat terrain can be described as terrain with small topographical changes and roughness variations e.g. trees, bushes and larger forest areas. In the non-flat areas or complex terrain, variations in the orography occurs. This could be mountains, hills, canyons etc. which all have substantial influence on the wind field (Manwell et al., 2010). For an extensive description of terrain classifications, the literature of Hiester and Pennell (1981) and Wegley et al. (1980) are recommended.

2.1.6 Available Power and Potential Energy

The potential energy in the wind can be explained by the flow of air (dm/dt) passing through a rotor disc with a swept area A (m^2). With the foundation in the continuity of fluid mechanics,

we can derive the mass flow rate as a function of air density ρ in (kg/m^3), air velocity U (m/s) with air density set to 1,225kg/m^2 (Manwell et al., 2010).

Which gives:

$$\frac{(dm)}{(dt)} = \rho AU \quad [2]$$

The available wind power (W): $$P = \frac{1}{2}\frac{(dm)}{(dt)}U^2 = \frac{1}{2}\rho AU^3 \quad [3]$$

The power output from a wind turbine (Derived from the turbines power curve):

$$P = \tfrac{1}{2}\rho AC_pU^3 \quad [4]$$

where C_p is the turbines overall efficiency also called power coefficient (turbine-, mechanical- and electrical efficiency.) In standard conditions, the wind power density is proportional to the density of the air. At sea-level the density is 1.225kg/m^3 with a temperature of 15˚C. Power from the wind is proportional to the swept area. The wind power potential is proportional to the third cube of the wind speed (Manwell et al., 2010). Following Betz`s Law, the maximum theoretical conversion of kinetic energy to mechanical energy is 16/27 or 59,3% (Rosvold & Hofstad, 2013).

2.2 Harvesting the Kinetic Energy

2.2.1 Wind Turbines and Wind Farms

The modern wind turbine is a highly sophisticated instrument which convert the kinetic energy in the wind to mechanical energy. A modern wind turbine Figure 5, is built up by a tower, a nacelle and a rotor (Hau & Renouard, 2013). The blades and rotor power the horizontal axel connected to the gearbox and generator inside the nacelle. The yaw alters the direction of the rotor and optimizing it with respect to the wind direction. The generator transforms the

mechanical energy to electrical energy which is connected to the local electrical gird (Hau & Renouard, 2013).

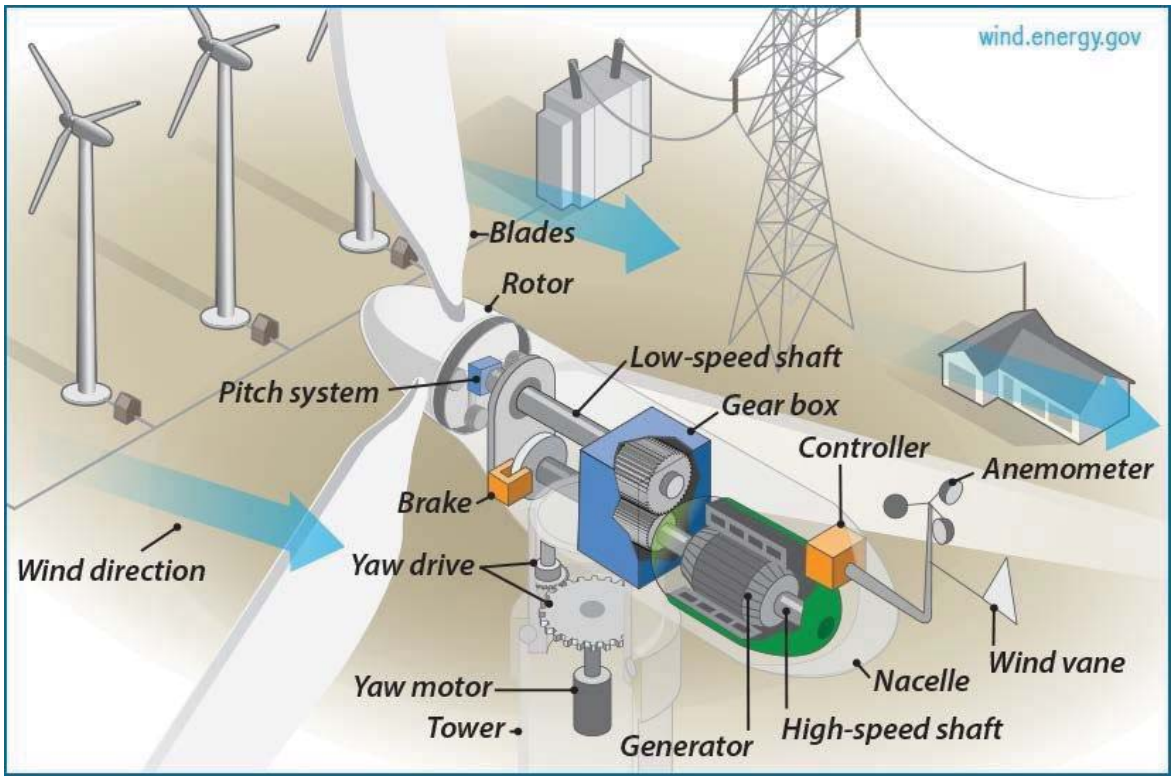

Figure 5 – Schematics of an horizontal axis turbine (US Department of Energy, 2018)

2.2.2 The Power Curve

The power produced by a wind turbine varies as the wind speed fluctuates. The power curve as seen in Figure 6 illustrates the relationship between the wind speed and the power output produced by a wind turbine. Traditional wind turbines will operate with a minimum cut-in wind speed for which the turbine will start producing energy. Rated speed is the wind speed where the generator delivers its maximum rated power output, and cut-out speed is a velocity limit set by the manufacturer. When the wind speed exceeds the cut-out limit the turbine will stop its production due to the risk of structural damages

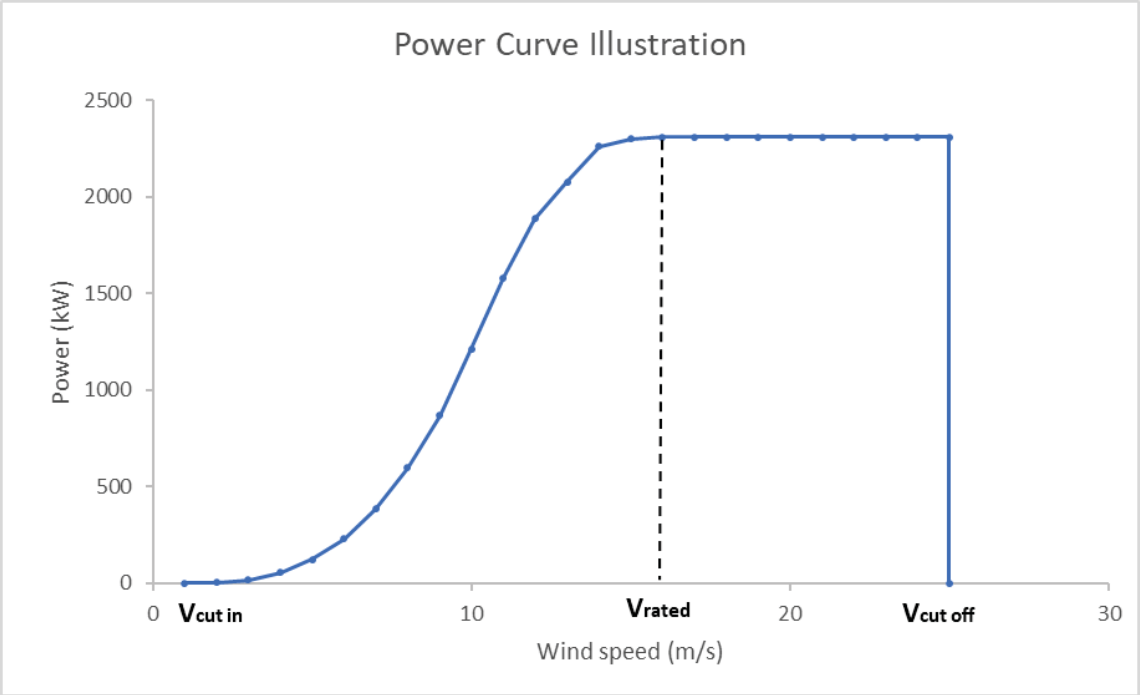

Figure 6 – Illustration of a wind turbine power curve

Wind power curves are usually described with two methods, theoretically or empirically (Manwell et al., 2010). Turbine manufacturers will provide a theoretical power curve which is based on what the turbine theoretically should produce under standard conditions. Sohoni et al. (2016) have analysed the limitations of deriving an accurate function that describes the realistic conditions at the turbine's location, and the findings implies that the use of empirical power curves will be more representative. The empirical method is based on actual site and turbine measurements. The power curve is described as a function of the produced power and measured wind speeds (Manwell et al., 2010).

2.3 Transmission System Operator

Statnett, which is owned by the Norwegian Department of Oil and Energy is responsible for the Norwegian power grid (Lont, 2018). Statnett as the TSO, is responsible of frequency regulation, maintenance, improving the efficient development of the power supply system, dealing with congestion and enabling international power trade (Lont, 2018). It is important for the operator to have good insight in predicted power production. In the case of imbalance, reserves must be activated to maintain the frequency. With increasing uncertainty in the

predicted power production, more reserves must be made available in situations with imbalance (Lont, 2018).

2.4 Wind Power Forecasting

Wind power forecasting is the work of predicting production estimates in variant time scales (minutes, days, year etc.) Today, power forecasts are primarily consisting of estimating a total production estimate for the upcoming hours or days. All tasks of estimating something that is powered by nature is a challenging undertaking. A forecast method applied on a selection of different wind farms does not necessarily need to produce the same results. The results could be varying depending on orography, terrain roughness, weather or even climate.

2.4.1 Wind Power Forecast Time Scales

There are various methods of classifying wind power forecasts in terms of time-scale, but there is no defined classification. By analysing the literature of Zhao et al. (2011) and Wang et al. (2011), the following classification of wind power forecasting could be proposed. The proposed categorizations with respect of time-scale and application is presented in table 1.
It is important to emphasise that the classification will vary depending on the applications.

Table 1 – Wind power forecast time scale classifications (Zhao et al. (2011) and Wang et al. (2011).

Time-scale	Range	Applications
Immediate – short- term	Seconds to one hour ahead	- Electricity market clearing - Regulation actions
Short – term	One hour to several hours ahead	- Load dispatch planning - Load increment/decrement decisions
Medium – term	6 hours to one week	- Day ahead electricity market - Intraday production
Long – term	One week to one year or more	- Electricity reserve requirements - Maintenance scheduling - Operational management - Feasibility study of wind farm design

2.4.2 Forecast Methods

With the work of predicting wind power, various methods are applied. Which method being applied could depend on accuracy, application and resources. The following three methods are primary methods used today.

I. Statistical and Learning Methods

The persistence approach is the simplest type of forecasting method. This method uses previous hours of wind speeds or power production to estimates for the forthcoming time steps (Barbosa de Alencar et al., 2017). The method assumes that there is a correlation between previous and future wind speeds. This approach is applied in the "Short-term" time forecasts with good results, but the precision of this forecasting method will decline with increased time frame (Milligan et al., 2003).

In more advanced statistical methods, the aim is to analyse historical data and search for the relationship between historical data and actual measurements (Foley et al., 2012). With increased computer science, the use of ANN together with learning methods, often referred to as artificial intelligence (AI) is becoming more prominent (Barbosa de Alencar et al., 2017).

This type of “black box” modelling establishes a statistical relationship between the selected input data and gives a potential power output from the wind farm (Foley et al., 2012). The learning methods allow the forecast to be tested against the actual measurements, and by doing so the model learns and improves the accuracy of the forecast (Kariniotakis et al., 2004).

II. Physical Approach

This method is based on developing physical models with input from advanced climatology data to produce wind speed and energy production forecasts. The physical method includes inputs such as orthography, blocking features, variations in terrain roughness, wind farm design and layout in their models (Wu & Hong, 2007). Models for site specific wind farms typically uses nesting to scale down meso - scale climate data from weather services to a spatial resolution of 10-15km (Kariniotakis et al., 2004). With the combination of metrological data and detailed description of the terrain, the output is a simulation of the physical movements of nature. CFD is an example of the advanced method of physical modelling. This method of modelling will be further described in chapter 2.5.

III. The Hybrid Approach

The hybrid approach combines forecasting methods. This could for example be using a combination of physical and statistical methods or short- and medium term models (Soman et al., 2010). In resent work, Castellani et al. (2016) used the method of combining ANN and CFD in a complex terrain scenario in Italy with promising results. The general idea of the hybrid approach is to combine the strengths of the different forecasting methods and obtain an optimal forecasting model with high accuracy (Wu & Hong, 2007).

2.4.3 Rapid Changes in The Wind

As mentioned earlier, the wind is unpredictable and stochastic of nature. Sudden variations in the wind can therefore cause rapid changes in the wind power output, and can therefore be demanding for the TSOs (Greaves et al., 2009). These variations are described in the literature as ramp up or down events (Greaves et al., 2009). The definition of a ramping event, as defined in Greaves et al. (2009), is a change in the wind farms power output which is at least 50% of the nominal power and occurs within a time frame of 4 hours or less.

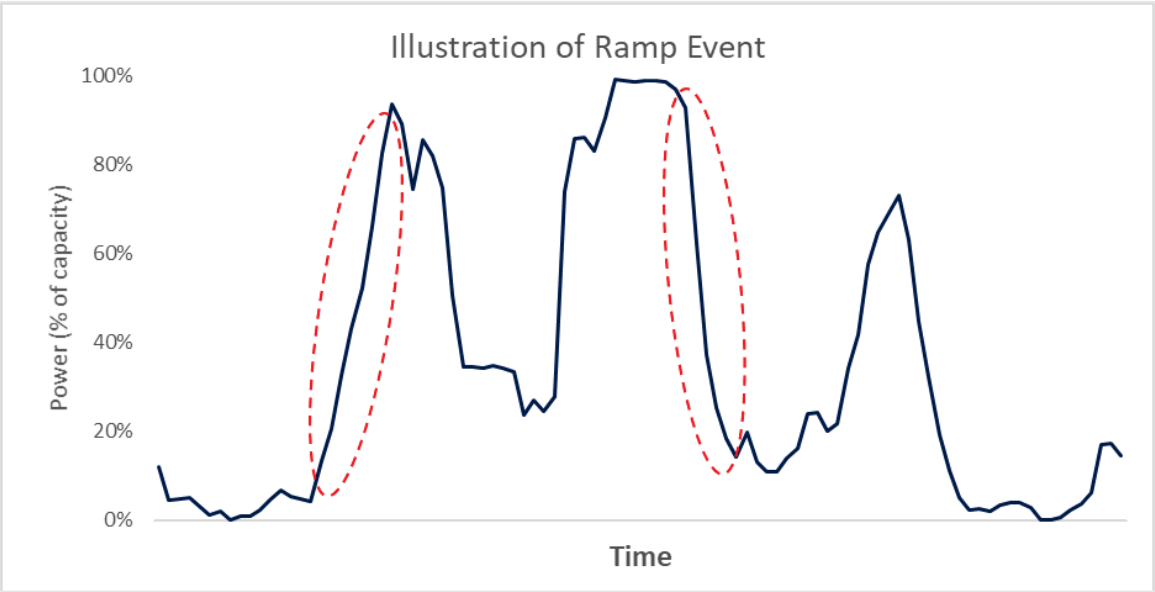

Figure 7 - Illustration of ramp up (Left circle) and ramp down (right circle). Inspired by Greaves et al. (2009).

2.5 Modelling the Physical World

CFD is a method where computer capacities meet the physical laws of fluid mechanics. CFD is used to analyse a system involving the flow of a fluid (either gas or liquid). The method has a wide range of use e.g. aerodynamics, marine engineering and hydrology (Versteeg & Malalasekera, 2007).

2.5.1 The Foundation of CFD

Fluid dynamics is the study of large motion of individual particles or atoms. The assumption is that even if the particle is infinitesimally small it is still possible to calculate mean velocity and mean kinetic energy. The vast number of particles or atoms is viewed upon as a continuous medium. In the human understanding of nature and its laws, the physical laws of conservation make up the building blocks of fluid dynamics.

Conservation Laws:

1. The conservation of mass
2. The conservation of momentum (Newton`s second law)
3. The conservation of energy

With this concept of modelling the flow field in an infinite area, the finite volume method is applied (Blazek, 2015).

2.5.2 Finite Volume Method

The finite control volume is based on the construction of an arbitrary finite region within the flow field. The establishment of a closed area with the control volume V and the control surface S allows us to either analyse the flow passing through the control volume, or we allow the control volume to move with the flow, illustrated in Figure 8 (Anderson & Wendt, 1995).

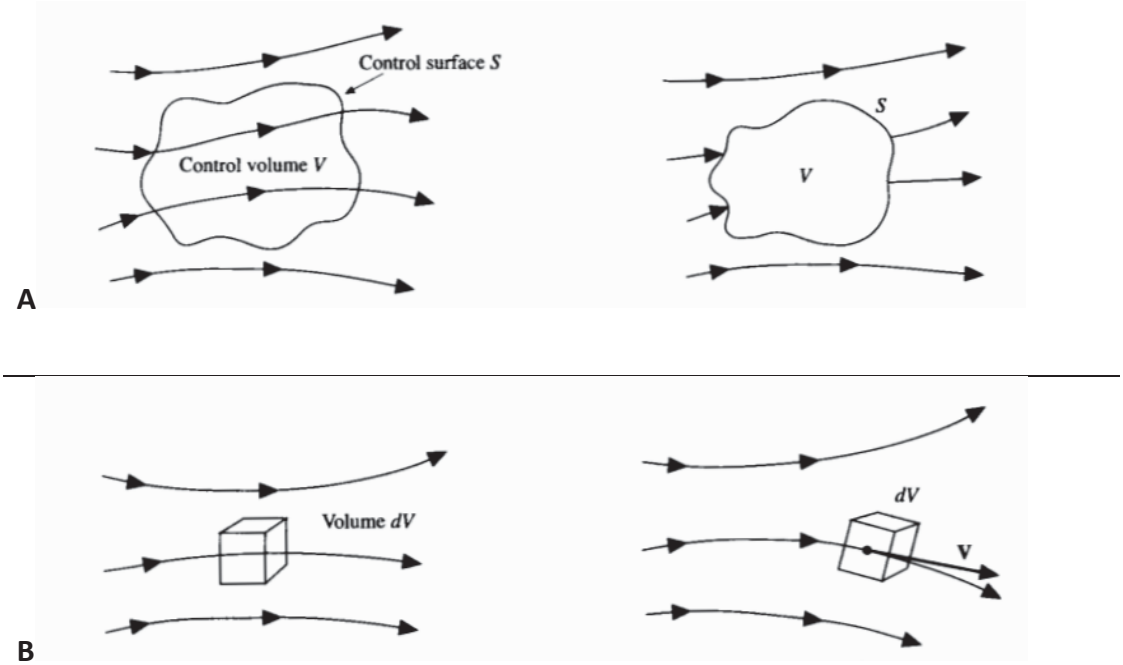

Figure 8 – A) The finite volume method. B) Infinitesimal fluid element (Anderson & Wendt, 1995)

2.5.3 Infinitesimal Fluid Element

With the concept of the infinitesimal fluid element being a continuous medium, it enables us to obtain dV (change in volume) of the fluid element instead of considering the flow as its whole (Anderson & Wendt, 1995). The principle of the volume being fixed, with the flow passing through or move together with the streamline would also apply here. In the latter case, the volume is moving along with the streamline with the velocity of vector V at a given point (Anderson & Wendt, 1995).

2.5.4 Navier - Stokes Equations

To describe the motion of fluids mathematically the Navier - Stokes equations, named after Claud-Louis Navier and Georg Gabriel Stokes, is applied. Five sets of non-linear partial differential equations are used to describe the motion of fluids (Versteeg & Malalasekera, 2007). Mass conservation, x-, y-, and z-momentum equations and energy equations are applied to derive a solution to the motion of the fluid (Versteeg & Malalasekera, 2007).

Solving the non-linear partial equations are done by combining mathematical equations with numerical approximation (Hervik, 2017). By applying an iterative method from computational mathematics, the solver generates a sequence of solutions which converges towards a solution satisfying the convergence criteria (Versteeg & Malalasekera, 2007).

2.6 WindSim

WindSim is a computational fluid dynamic software developed to simulate wind flows in different domains. WindSim was originally developed to simulate local wind fields along the Norwegian Coast under the establishment of the Norwegian Wind Atlas. Today, WindSim has been applied on a broad variety of complex wind flow simulations. The foundation for the simulations is the Reynolds Average Navier Stokes (RANS) equation. The solver utilizes the computational engine Phoenics to create a numerical solution that represents the real world.

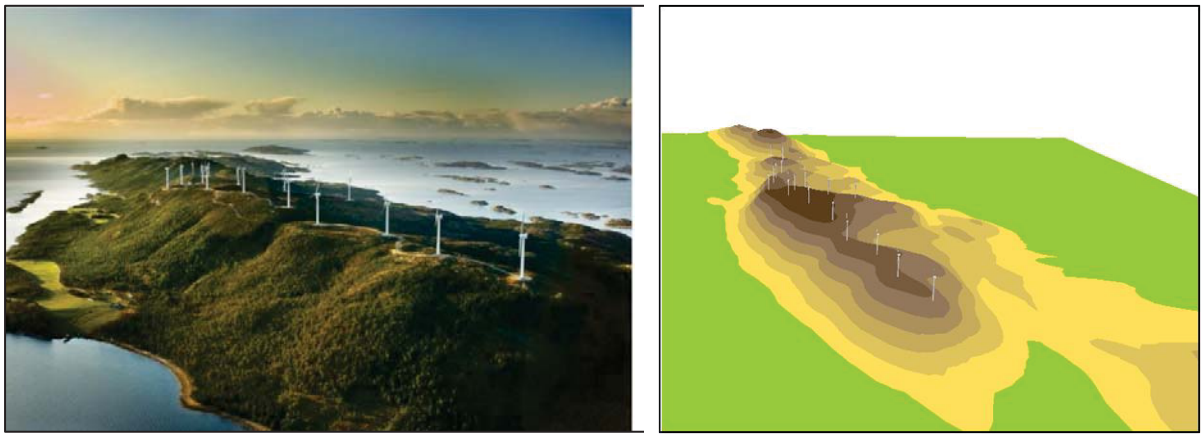

Figure 9 – Basic Course – WindSim. Real world vs. terrain model (3D) (Gravdahl, 2019)

2.6.1 The Approach

The simulations in WindSim are built on six modules, *Terrain*, *Wind Fields, Objects, Results, Wind Resources and Energy*. The three first modules needs to be completed in the given order, while the three last could be completed in an arbitrary order, depending on desired application. In the *Terrain* module the simulation- and area of interest will be defined. The aim is to generate a 3D model of the simulated area with all the components that could influence the wind flow. These components could be roughness, elevation, obstacles and forest. A refinement of the mesh grid will be focused towards the centre of the area of interest. If you increase the resolution of the cells in x-, y- and z-direction the refinement increases the precision in the focus area. In the second module, the *Wind fields* are estimated. The program calculates the wind fields for each wind sector in 360 degrees. The program corrects the wind flow for terrain effects and establishes a wind database. The *Objects module* enable the users to place turbines, import wind measurements, import climatologies and to inspect the layout in a 3D viewer. Based on the estimations of the wind fields the *Results* module will present the results for the simulation area. This includes wind speeds, turbulent intensity and directional vectors. Furthermore, in the *Wind resources module* the results are scaled with the climate information provided by the met mast or imported climatology data. The model then estimates a wind resource map for the area. In the final module, *Energy,* the total and per turbine AEP will be estimated. The numerical parameters of the wind flow will also be presented. (Extended information about WindSim methodology could be found at: www.windsim.com)

3 Models, Data and Methodology

This chapter will describe the wind farms analysed, present the foundation and describe the models and software that have been applied. The main purpose of chapter 3 is to provide insight into to how the work has been conducted and describing the methods which have been applied.

3.1 The Wind Farms

The following five wind farms have been analysed: Smøla, Hitra, Valsneset, Bessakerfjellet and Ytre Vikna. The wind farms are located in the middle of Norway, in Møre and Romsdal and Trøndelag county. All the wind farms are placed in the outer coastal regions due to the prominent wind resources found along the Norwegian coastline. Smøla is the oldest wind farm, which became operational in 2002. Hitra was established in 2004, Valsneset in 2006, Bessakerfjellet in 2008 and Ytre Vikna in 2012. The vegetation of the sites is dominated by thin vegetation and boreal coniferous forests while the terrain is of varying characteristics.

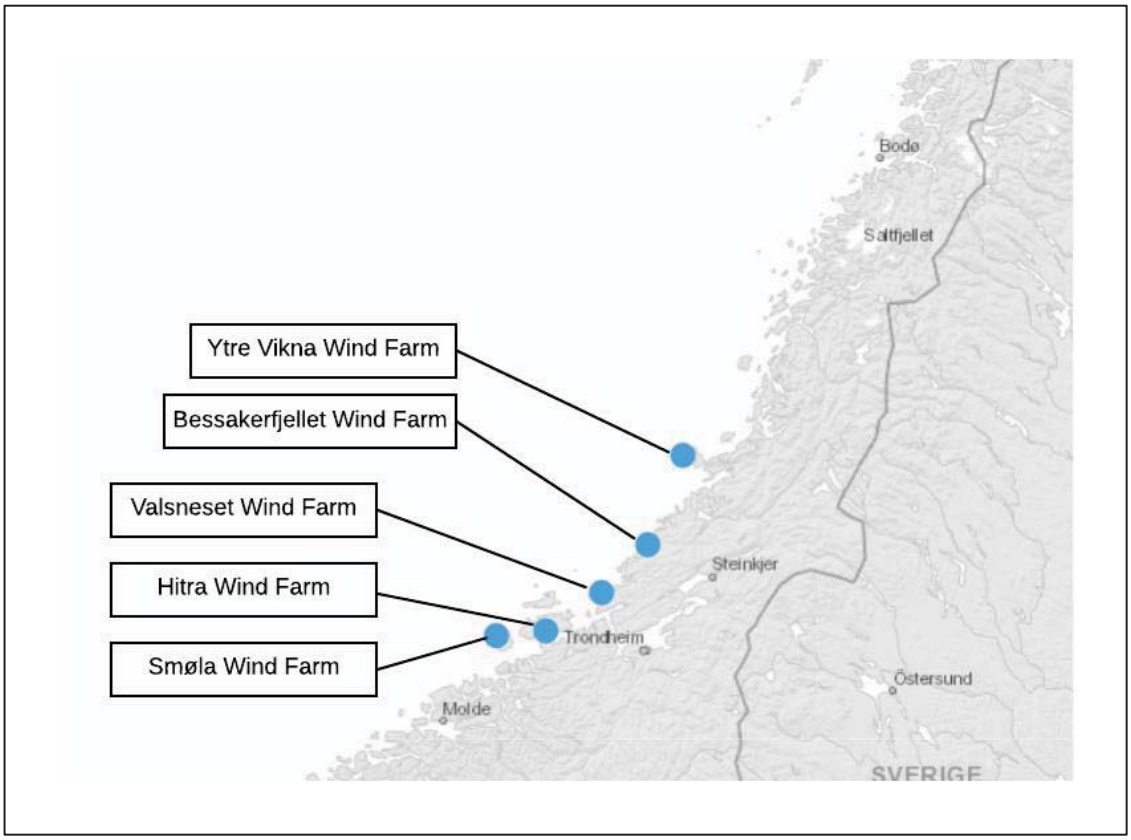

Figure 10 – Location of the wind farms (NVE Atlas, 2019)

3.2 Data Foundation

The data foundation for this project is based on data publications from the Norwegian Metrological Institute and NVE.

3.2.1 Norwegian Metrological Institute and Yr.no

Yr is one of the largest weather forecast providers in Europe. Their services are a cooperation between the Norwegian Metrological Institute and the Norwegian Broadcasting Company (NRK) owned by the Norwegian Government (Jensen Støver, 2019). As a part of their services, Yr publishes climatology data free to access for the public. WindSim has collected the forecasted wind speeds and direction for the five wind farms over a longer period as part of their wind power forecasting services. The development of the time series is done by downloading climatology data in "day ahead" mode. To obtain the forecast for the next day, they remove the forecasted windspeed between time of the forecast estimation and until the time of the wanted forecast. If the time is 06:00 today, 18 hours are removed, this produces a forecast for the next 24-hours.

The complete time series stretches from 2016-12-21 00:00 to 2018-01-24 23:00. The forecasted windspeeds are given on an hourly basis with the corresponding wind direction in degrees (0-360˚). It is important to emphasize that the wind speeds and directions are based on a forecast and not actual measurements. The coordinates for the forecast at the five wind farms sites are based on the park placement coordinates provided by the NVE geographical atlas. For this project, the time series for the period 01.01.2017 – 00:00 to 30.12.2017 – 23:00 is extracted into separate time series for each of the wind farms. Table 2 exemplifies three of the first entries in the time series. From 01.01.2017 – 00:00 to 01.01.2017 – 02:00 for Smøla wind farm.

Table 2 – The three first entries in the times series for Smøla wind farm

rec nr:	year:	mon:	date:	hour:	min:	dir:	speed: (m/s)
1	2017	1	1	0	0	320.8	6.4
2	2017	1	1	1	0	347.3	9.8
3	2017	1	1	2	0	335.9	10.9

3.2.2 Norwegian Water Resource and Energy Directorate

NVE publishes a wind power production report for Norwegian wind farms annually on their web page. The report has been published continuously since 2007, and they report the development in Norwegian wind power, production, new instalments, performance indicators and time series with data of hourly power production for all the Norwegian wind farms. The foundation for these time series, are the electric output that wind farms delivers to the grid, which is monitored and owned by the Norwegian grid operator Statnett.

The complete time series from NVE covers the period from 01.01.2002 - 00:00 to 31.12.2017 – 23:00 with an hourly power production in MWh for each wind farm. To synchronize the predicted Yr data with the observed data from NVE, the period 01.01.2017 – 00:00 to 30.12.2017 – 23:00 is extracted and divided into five datasets. Table 3 displays the three first entries in the NVE time series all the wind farm`s.

Table 3 – The three first entries in the NVE time series

Rec	Date and Time	Ytre Vikna (MWh)	Smøla (MWh)	Hitra (MWh)	Valsneset (MWh)	Bessakerfjellet (MWh)
1	01/01/2017 00:00	3.744	103.820	38.069	8.700	17.782
2	01/01/2017 01:00	12.480	90.910	36.572	8.390	31.861
3	01/01/2017 02:00	17.184	72.310	32.934	8.680	28.345

3.2.3 Synchronizing the Datasets

In the time series from Yr, 24 hours of data were missing on four dates: 07/04, 06/06, 04/07 and the 30/10 for all the wind farms, the forecast for Ytre Vikna was also missing one additional day 20/07. All the missing time steps are flagged as "invalid" in the data sets from NVE, and in the theoretical production and the predicted turbine production from WindSim in Windographer. The flagging-tool excludes the time steps from the statistical analysis and graphical visualization. Figure 11 illustrates the process of excluding the missing data at 07.04.2017 for Bessakerfjellet wind farm. Based on this information, the finished datasets from Smøla, Hitra, Valsneset and Bessakerfjellet consists of 8640 valid entries and Ytre Vikna consists of 8616 valid entries.

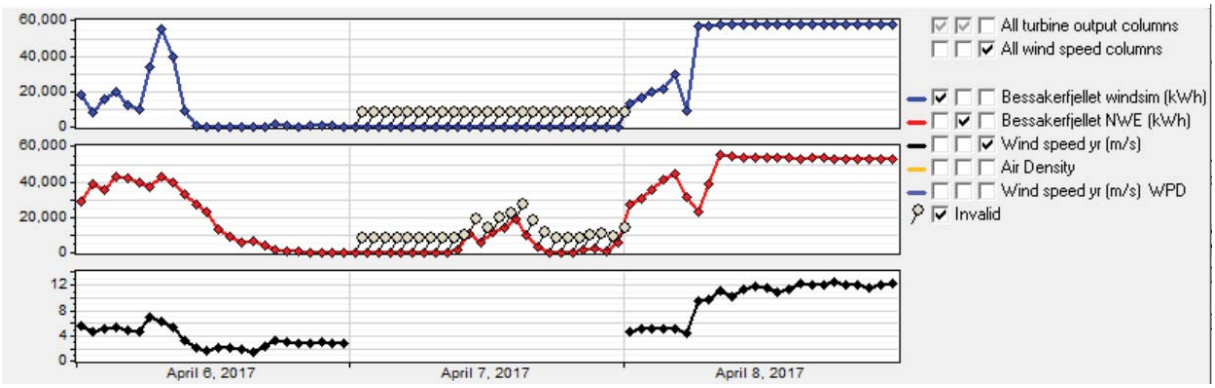

Figure 11 – Snippet of flagged time steps as "invalid" in Windographer.

3.3 The Forecasting Methods

To categorize the two methods applied, they have been named Strategy I "*Wind to Power*" and strategy II is called "*Wind + CFD to Power".* A visual representation of the two methods are illustrate in Figure 12.

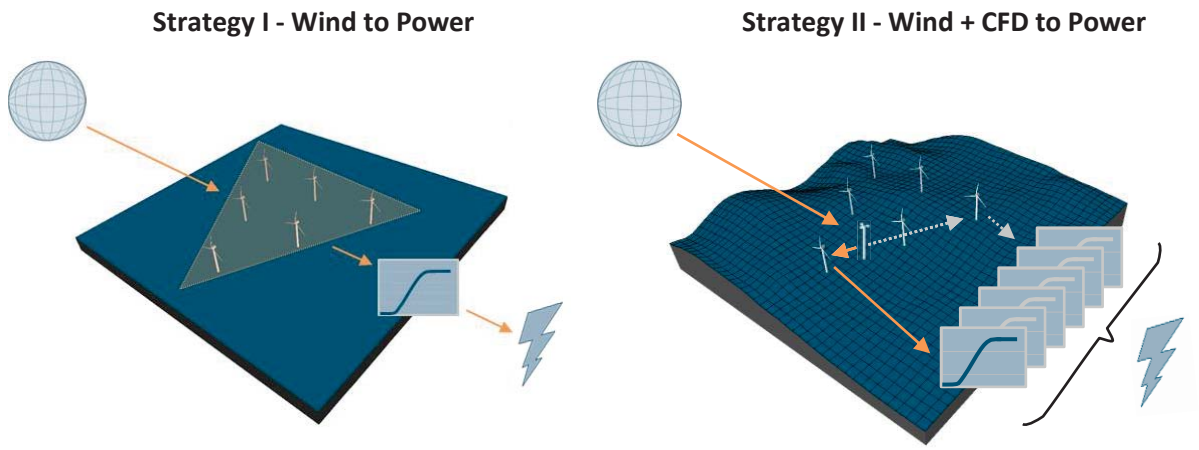

Figure 12 – Graphical description of the two forecasting methods

Strategy I – *Wind to Power* utilizes the Yr time series at the selected wind farms location as input. The method does not utilize the wind direction, only wind speeds are applied. By combining the time series with the theoretical wind turbine power curve, the wind power production forecast is estimated. The power production for the theoretical power curve is then multiplied with the respective number of turbines installed at the wind farm. The result is a power production forecast for the whole wind farm.

Strategy II – *Wind + CFD to Power,* is a more complex forecasting method. The *Wind to Power* method only relies on wind speed as input, the *Wind + CFD to Power* method utilizes the wind fields. By introducing CFD to the model, the method accounts for the physical aspects of the simulation area by deriving a numerical representation of the selected area and includes the effects on the wind flow caused by the terrain. As a result, the model estimates power production per turbine and calculates a total production for the wind farm.

3.4 Linear Interpolation of The Power Curve

The statistical produced wind power forecast has been estimated by using the forecasted wind speed and an equivalent power curve for the selected wind farm. The theoretical power curves for the different wind farms could be found in Appendix A. To derive a continuous function of the power curve and estimate the power output between bins, linear interpolation is used (Aarnes & Aubert, 2018).

Linear Interpolation solving for y:

$$y = y_0 + (x - x_0)\frac{y_1 - y_0}{x_1 - x_0} = \frac{y_0(x_1 - x) + y_1(x - x_0)}{(x_1 - x_0)} \quad [5]$$

With the work of calculating the power output for each forecasted wind-speed a function is written in Excel. The function derives the power output with the use of the *Forecast, Offset* and *Match* function. Figure 13 exemplifies how two points have been interpolated for the Enercon E70 2.3 MW turbine at Bessakerfjellet.

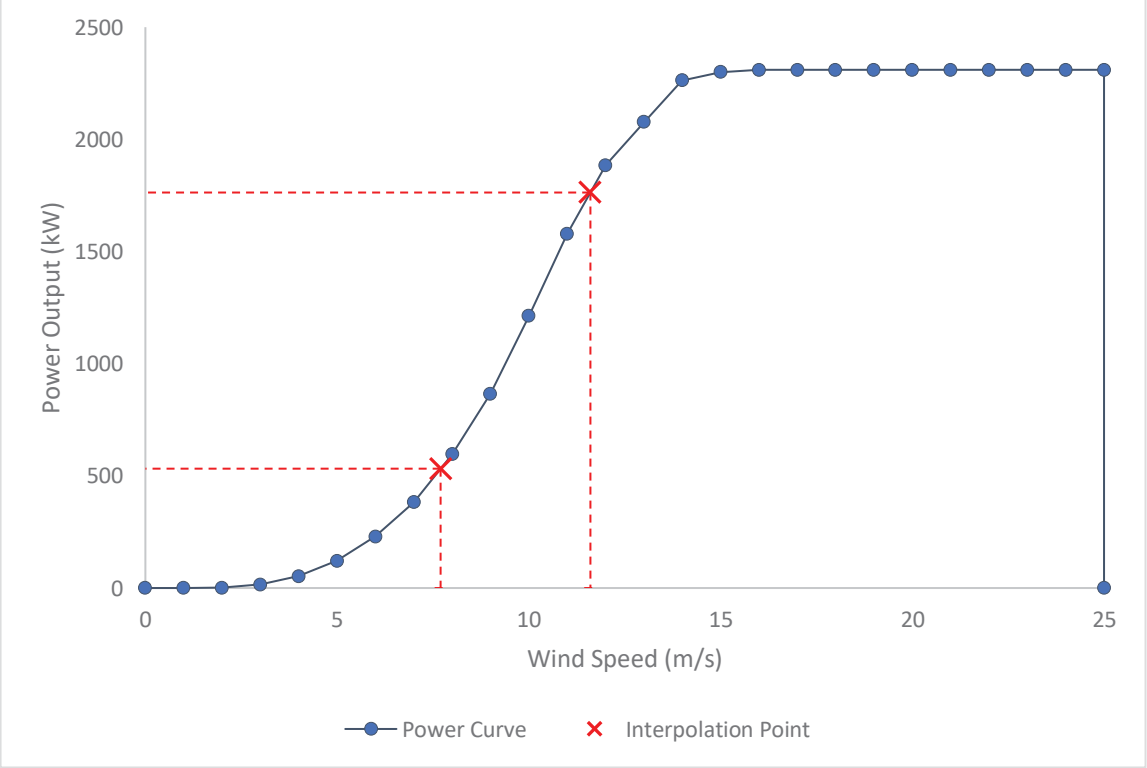

Figure 13 – Interpolation between wind speed bins

3.5 Windographer

With the work of processing and analysing the exported time series, Windographer is utilized. Windographer is a professional software used for analysing, visualizing and validating time series and wind resource data in wind farm projects. The program has been used in combination with Microsoft Excel to analyse the estimated power data. (Extended information could be found at: www.windographer.com)

3.6 Designing the Wind Farms in WindSim

The work of designing the wind farms in the simulation software WindSim has been done in compliance with recommendations established by WindSim. In the following chapters, a selection of important aspects of the models will be clarified. Appendix B provides an extensive report for all the wind farm`s design and layout. With the module-based layout in WindSim, *Terrain, Wind Fields and Objects* are required to be completed in the respective order. In the last module, *Energy* is estimated to produce the needed production data report for the analysis. The process of designing and running the CFD simulations have been conducted for all the wind farms described in this project.

3.6.1 Terrain

Terrain is the first step in the work of building the model. The objective is to establish the horizontal and vertical area to simulate. In the work of creating the simulation domain, the program WindSim Express 9.0 (WSE) is used to establish the .gws file which contains information about the terrain, elevation and roughness height. Having created the .gws file, the processes of establishing CFD-model in WindSim 9.0.0 can commence with the terrain module. To define the elevation and roughness height in the simulation area, ASTER GDEM v2 Worldwide Elevation Data (1 arc-second Resolution) is used for the elevation data and for the roughness height, CORINE Land Cover Europe 2006 (100 m Resolution) is applied. Forest modelling has been disregarded and smoothing of the terrain is not applied.

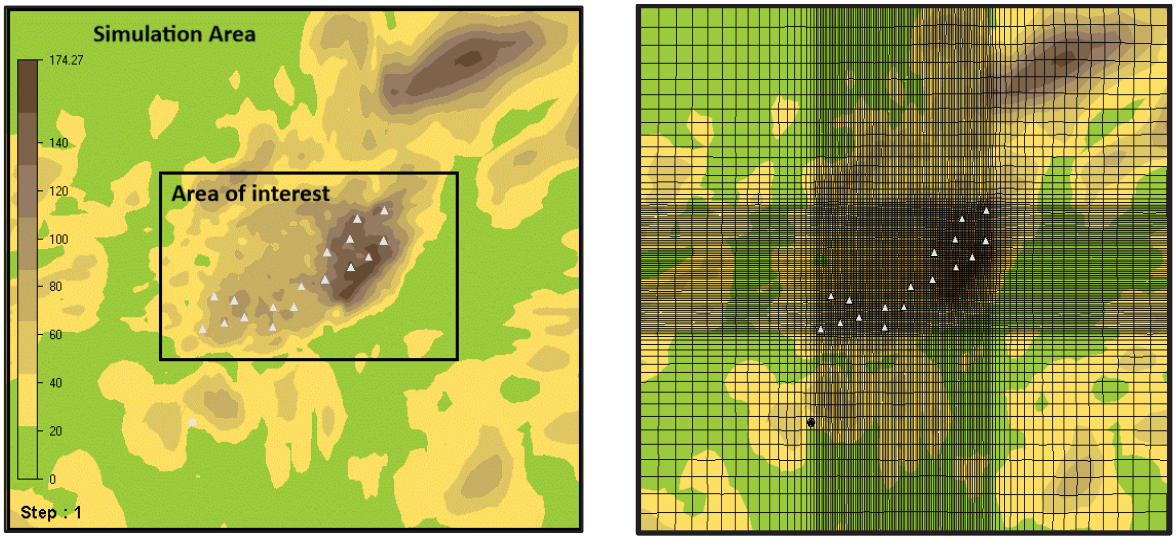

Figure 14 – Digital terrain model (left) and refinement area (right) of Ytre Vikna. Turbine placement visualized with triangles

In the process of adjusting the boundaries of the simulation area, inclusion of all terrain features that potentially could influence the wind flow is important. For example, excluding of important orographic features could have impact on the wind field. For this project the limit of 500 000 cells were used to establish the numerical model. Gridding and refinement area were optimized and completed automatically by WindSim.

Vertical gridding is of great relevance in the work of capturing the effects caused by the terrain. This is done by gradually refining the grid in z-direction towards the ground. In the five models, the work of obtaining at least 6-8 cells in the first 100m which is recommend by Gravdahl and Meißner (2015) were attempted and successfully accomplished.

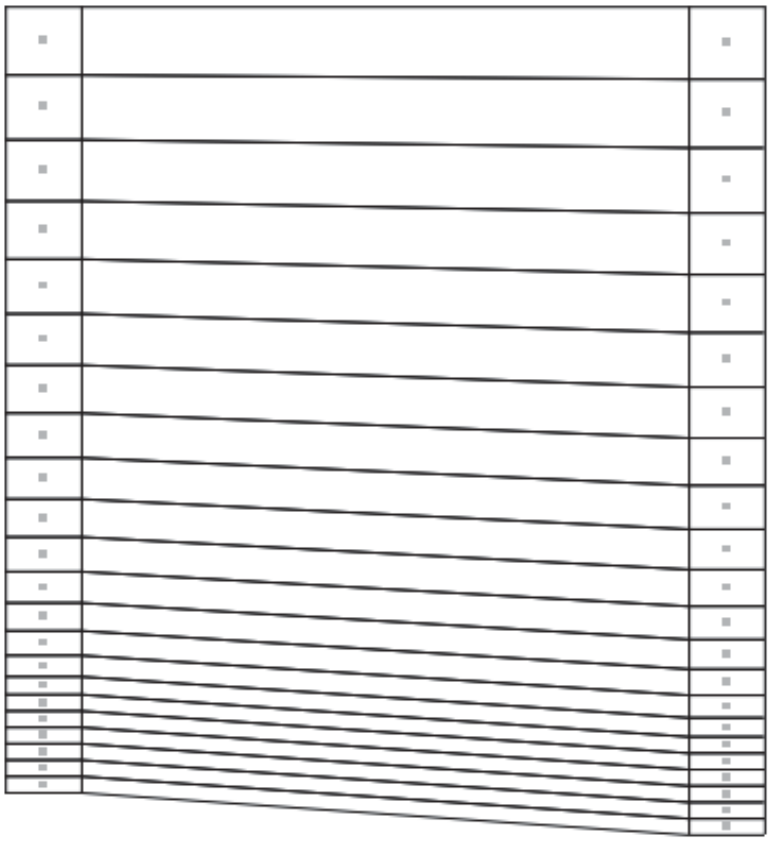

Figure 15 – Example of refinement in the vertical z-direction for Smøla wind farm

3.6.2 Wind Fields

With the terrain being established, the next step is to determine the wind field in 0-360˚. By solving the RANS equation, the wind field is calculated in 36 sectors. The number of iterations is set to 500 and the convergence criteria is 0,001. Defining the boundary layer height and avoiding risks of unrealistic wind flows, the recommended setting of 500m and a wind speed of 10 m/s is applied to the upper boundary layer conditions. To determine the effects of turbulence, the standard k-epsilon turbulence modelling is used and the air-pressure for the sites are set to standard (1.225kg/m^3).

3.6.3 Objects

For the placement of the turbines, the coordinates have been collected from the geographical database provided by NVE. The database contains information about the placement of all turbines in Norwegian Wind Farms, the turbine coordinates are imported into WSE.

The placement of the climatology points is the same as the placement-coordinates for the wind farm found in the NVE atlas. The height of the climatology is set to 10m as a default for all the sites. After placing the met-mast, WindSim then estimates the wind flow at each turbine placement.

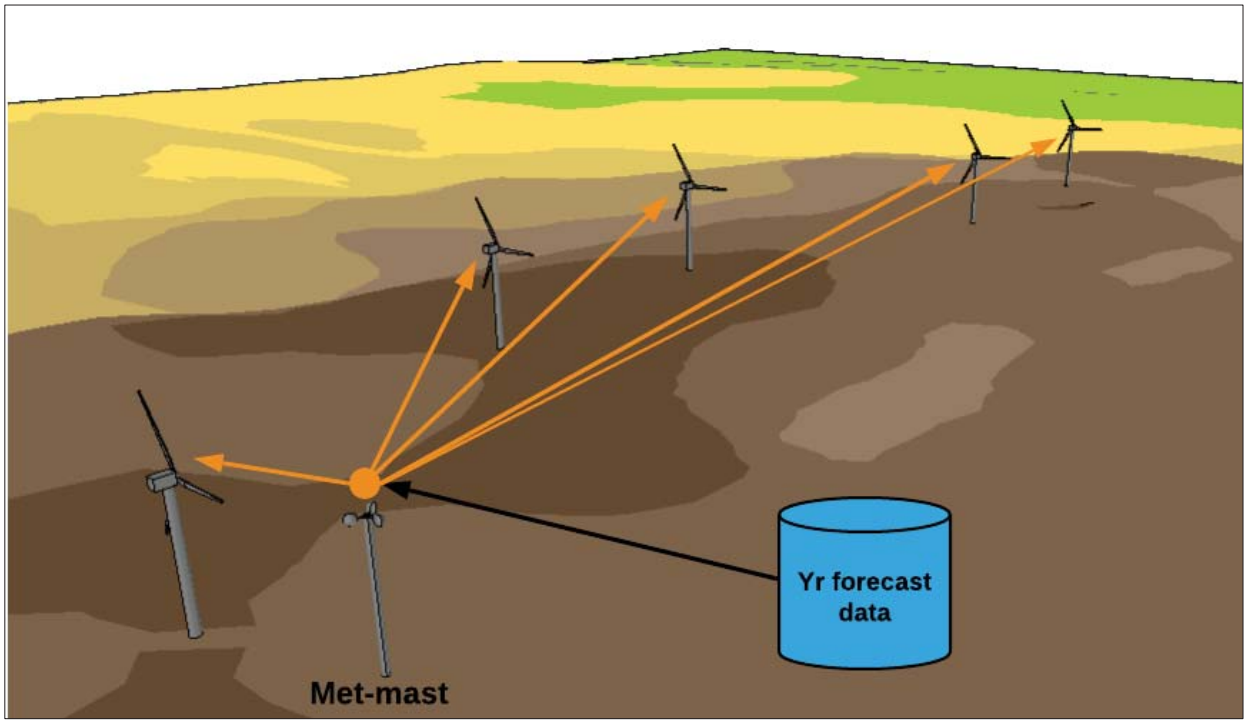

Figure 16 – Wind flow calibration for each turbine

The selected wind farms have installed a variety of turbines. To give an accurate representation of the actual wind farm, information about the specific turbine selection has been collected from the published NVE report (Weir, 2013). Table 4 display the various turbine models found at the different wind farms. The corresponding effect curves are presented in Appendix A. Note that Smøla wind farm consists of two building steps. Step 1 consists of 20 Bonus 2.0 MW 76 and step 2 consists of 48 Bonus 2.3 MW 82 turbines.

Table 4 – Selected wind turbines

Wind Farm	Turbine
Hitra	Bonus 2.3 MW 82
Smøla	Step 1: Bonus 2.0 MW 76* Step 2: Bonus 2.3 MW 82*
Bessakerfjellet	Enercon E-71 2.3 MW
Valsneset	Enercon E-71 2.3 MW
Ytre Vikna	Enercon E-70 2.3 MW

** The manufacturer of Bonus wind turbines was acquired by Siemens in 2004 (Hoel, 2004)*

3.6.4 Energy

In the final step the annual energy production for the wind farm is calculated. The total energy output is calculated based on the selected climatologies imported in *Objects*. By exporting the power history, WindSim generates a .csv file with the hourly production per turbine and as for the total wind farm. The file is exported and post-processed in Windographer and Microsoft Excel.

3.7 Benchmarking and Uncertainty Analysis

With the work of evaluating the performance of the forecasting strategies, Mean Absolut Error (MAE) have been chosen for this project. The MAE is a commonly used error measurement, and its measures the average magnitude in a set of predicted values (Willmott & Matsuura, 2005). The MAE has then been normalized against the nominal power of the wind farm, enabling the possibility of comparing the different wind farms analysed in this project.

$$\mathrm{NMAE} = \frac{1}{GN}\sum_{i=1}^{N}|\hat{y}_i - y_i| \qquad [6]$$

Where *N* is the number of values in the dataset, $\hat{y}_i$ is the predicted value, y_i is the observed value and *G* is the nominal power of the wind farm.

4 Results

In this chapter, the results from applying the two forecasting methods: *Wind to Power* and *Wind + CFD to Power* will be presented. The forecasted power production and the performance of the forecast will be presented on a monthly time-scale for the two strategies. In the final part of this chapter, an analysis of the vertical height (z-direction) of the calibration point at Bessakerfjellet have been investigated. Finally, some short time series of interest will be presented, this is done to highlight some of the challenges of wind power prediction with forecasted wind speeds.

4.1 Bessakerfjellet

4.1.1 Overall Production Forecast

For Bessakerfjellet wind farm, forecasting strategy I – *Wind to Power* estimated a total production of 77,050.93 MWh. Strategy II – *Wind + CFD to Power* estimated it to be 200,486.62 MWh. The forecasted power predictions and the observed production is presented in Figure 17 on a monthly time-scale.

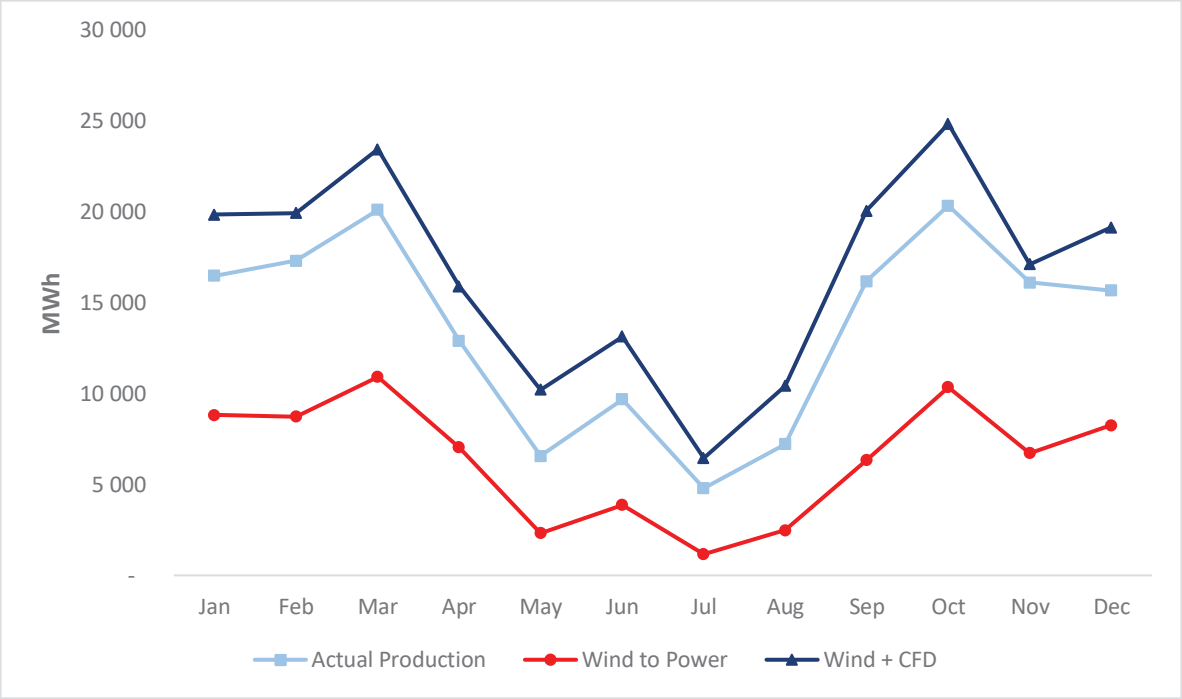

Figure 17 – Production forecast Bessakerfjellet

The historical data provided by NVE give a total production of 163,377.88 MWh for the forecasting period. The results show that strategy I underestimates the total production with 86,326.96 MWh, while strategy II overestimates the total production with 37,108.74 MWh over the total period.

4.1.2 Forecast Error

Measuring the performance of the two strategies, *Wind to Power* have a NMAE of 19.19% and strategy II – *Wind + CFD to Power* presents a NMAE of 16.56%. For Bessakerfjellet, the forecasting method, which includes CFD, presented a lower forecasting error compared to *Wind to Power*, being 2.63% lower. Figure 18 visualises how the error measurement varies during the forecast period.

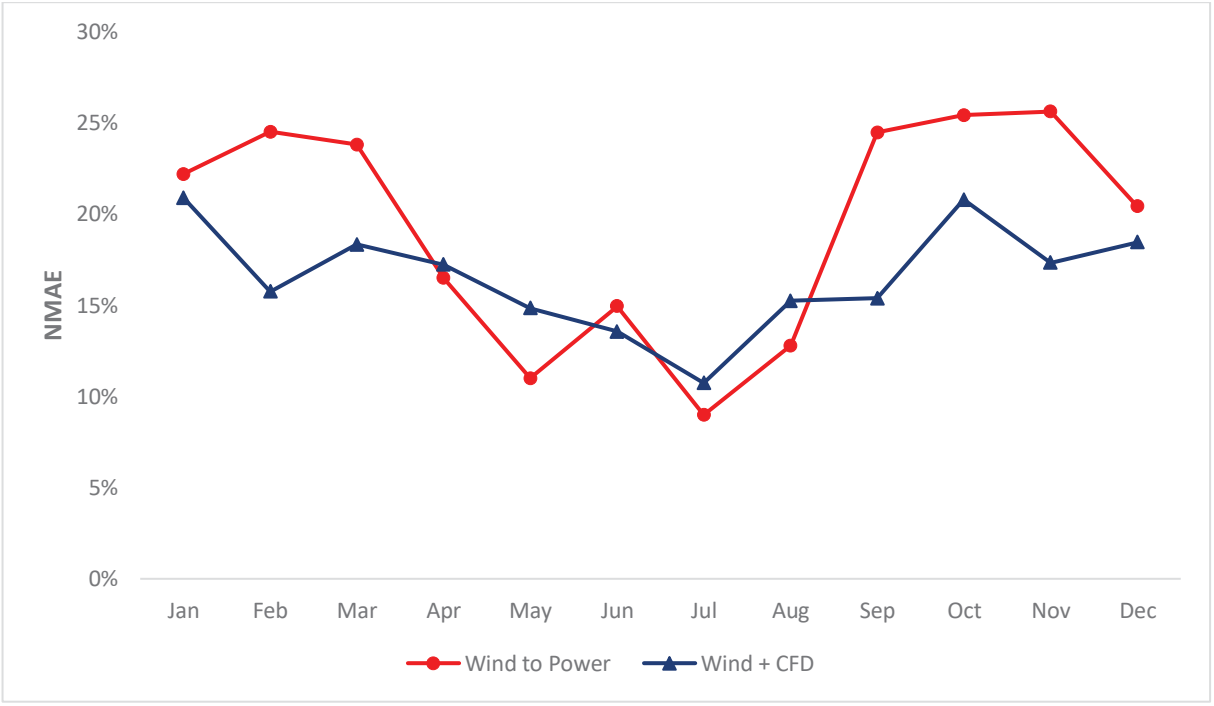

Figure 18 – Forecast error Bessakerfjellet

4.2 Hitra

4.2.1 Overall Production Forecast

For Hitra wind farm, forecasting strategy I – *Wind to Power* estimated a total production of 54,249.99 MWh. Strategy II – *Wind + CFD to Power* estimated it to be 163,449.68 MWh.

The forecasted power predictions and the observed production is presented in Figure 19 on a monthly time-scale.

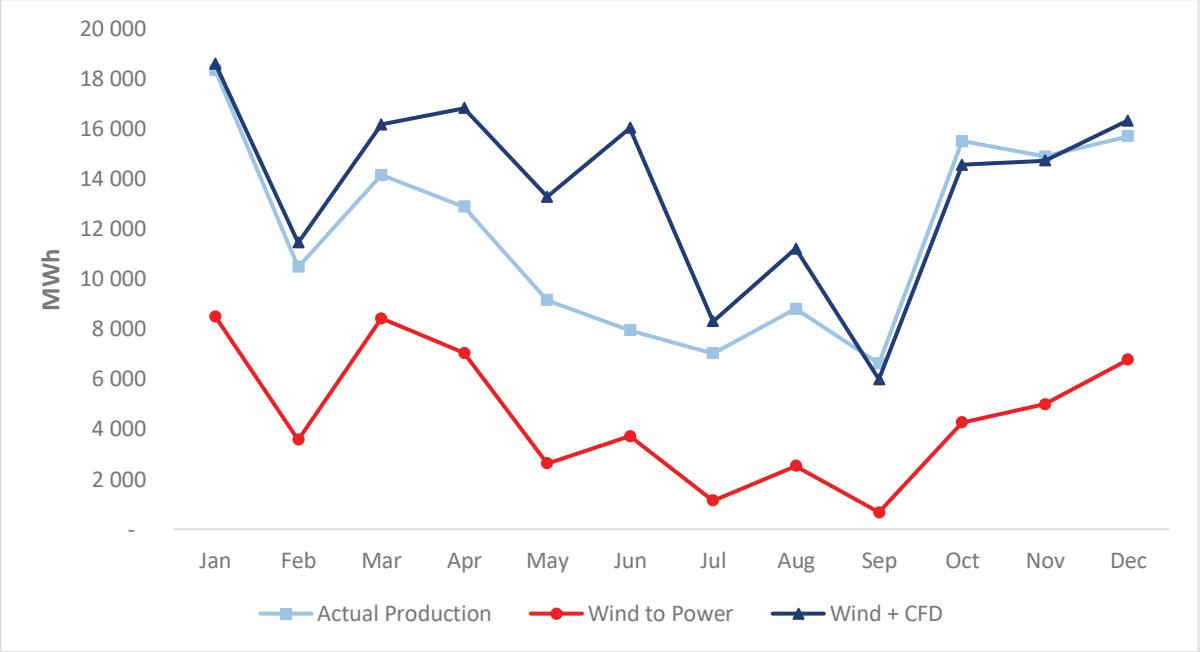

Figure 19 – Production forecast Hitra

The historical data provided by NVE give a total production of 141,489.59 MWh for the forecasting period. The results show that strategy I underestimates the total production with 87,239.61 MWh, while strategy II overestimates the total production with 21,960.09 MWh over the total period.

4.2.2 Forecast Error

Measuring the performance of the two strategies, *Wind to Power* have a NMAE of 21.06% and *Wind + CFD to Power* presents a NMAE of 16.64%. For Hitra wind farm, the forecasting strategy which includes CFD presented a lower forecasting error compared to *Wind to Power* with 4.42%. Figure 20 visualises how the error measurement varies during the forecast period. Note the sudden change in performance for the CFD method in June.

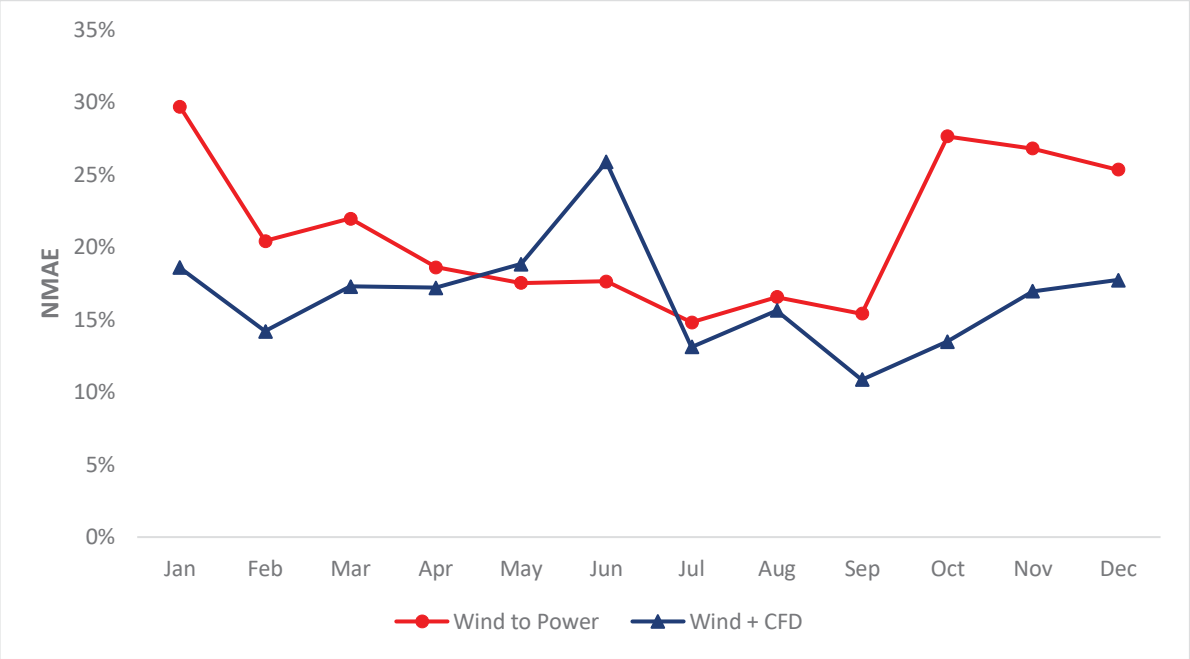

Figure 20 – Forecast error Hitra

4.3 Smøla

4.3.1 Overall Production Forecast

For Smøla wind farm, forecasting method I – *Wind to Power* estimated a total production of 282,691.09 MWh. Strategy II – *Wind + CFD to Power* estimated it to be 463,592.97 MWh. The forecasted power predictions and the observed production is presented in Figure 21 on a monthly time-scale.

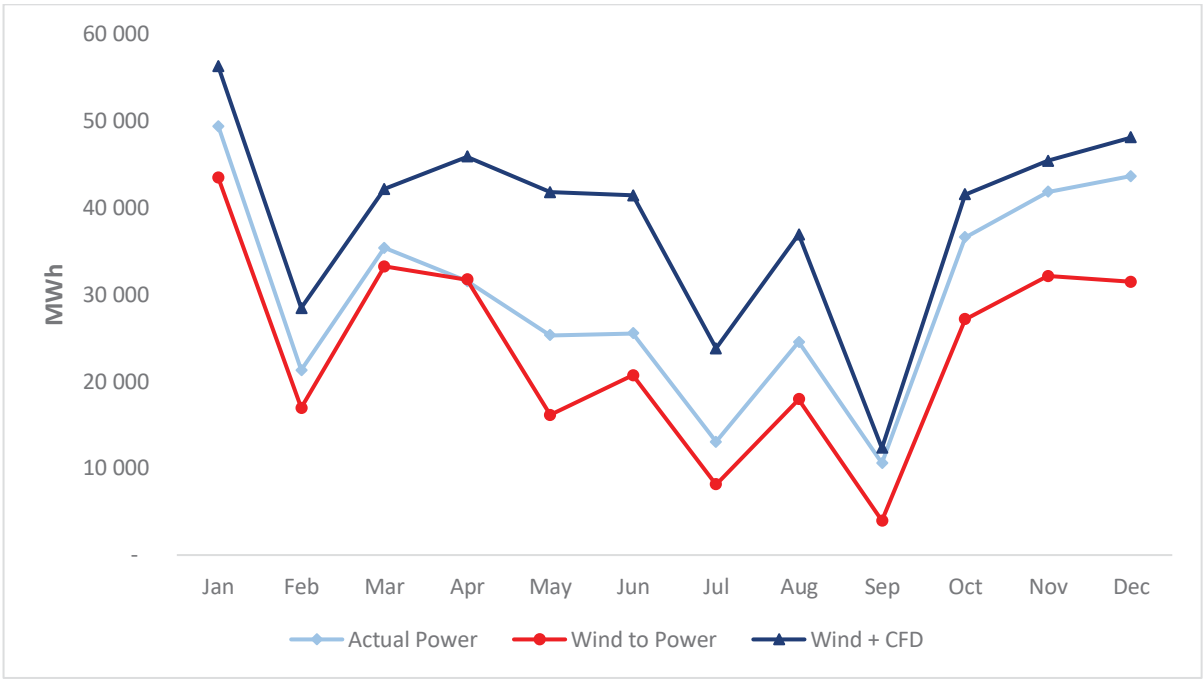

Figure 21 – Production forecast Smøla

The historical data provided by NVE give a total production of 358,280.50 MWh for the forecasting period. The results show that method I underestimates the total production with 75,589.41 MWh, while method II overestimates the total production with 105,312.47 MWh over the total period.

4.3.2 Forecast Error

Measuring the performance of the two strategies, *Wind to Power* have a NMAE of 13.21% and *Wind + CFD to Power* presents a NMAE of 17.80%. For Smøla wind farm, the forecasting method using the theoretical power curve produced the forecast with the lowest error measurement with a difference of 4.59%. Figure 22 visualises how the error measurement varies during the forecast period. The *wind + CFD* systematically overestimates the production from February to October, which can be seen by the large increase in the forecasting error.

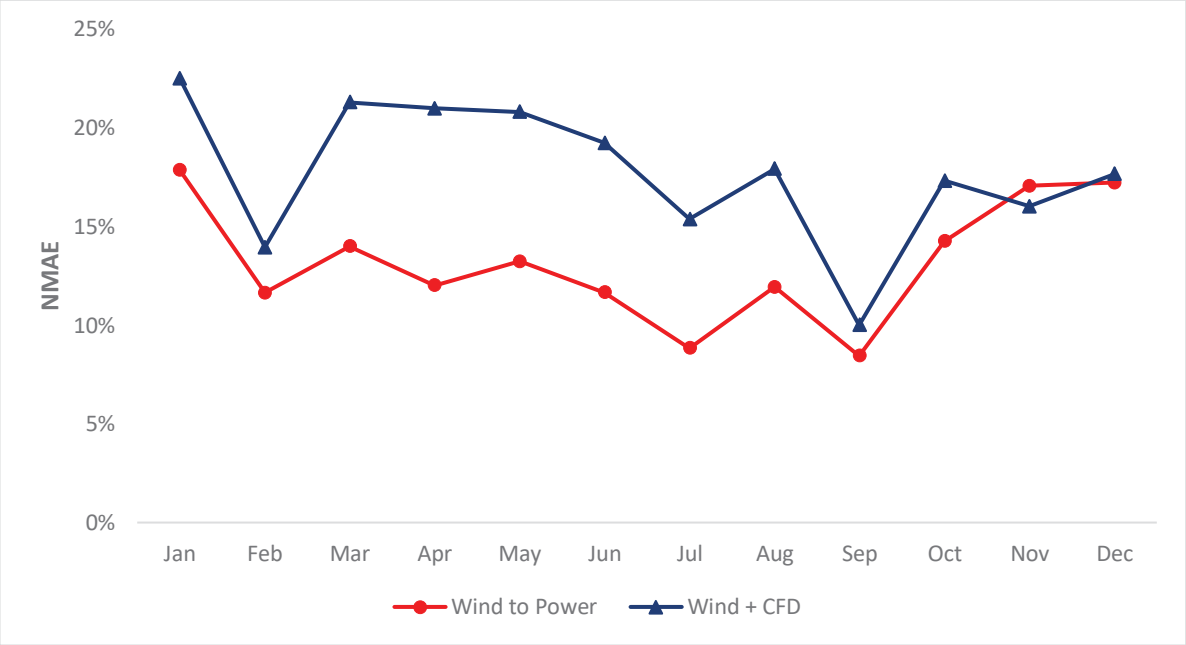

Figure 22 – Forecast error Smøla

4.4 Valsneset

4.4.1 Overall Production Forecast

For Valsneset wind farm, forecasting strategy I – *Wind to Power* estimated a total production of 20,170.12 MWh. Strategy II – *Wind + CFD to Power* estimated it to be 30,147.91 MWh. The forecasted power predictions and the observed production is presented in Figure 23 on a monthly time-scale.

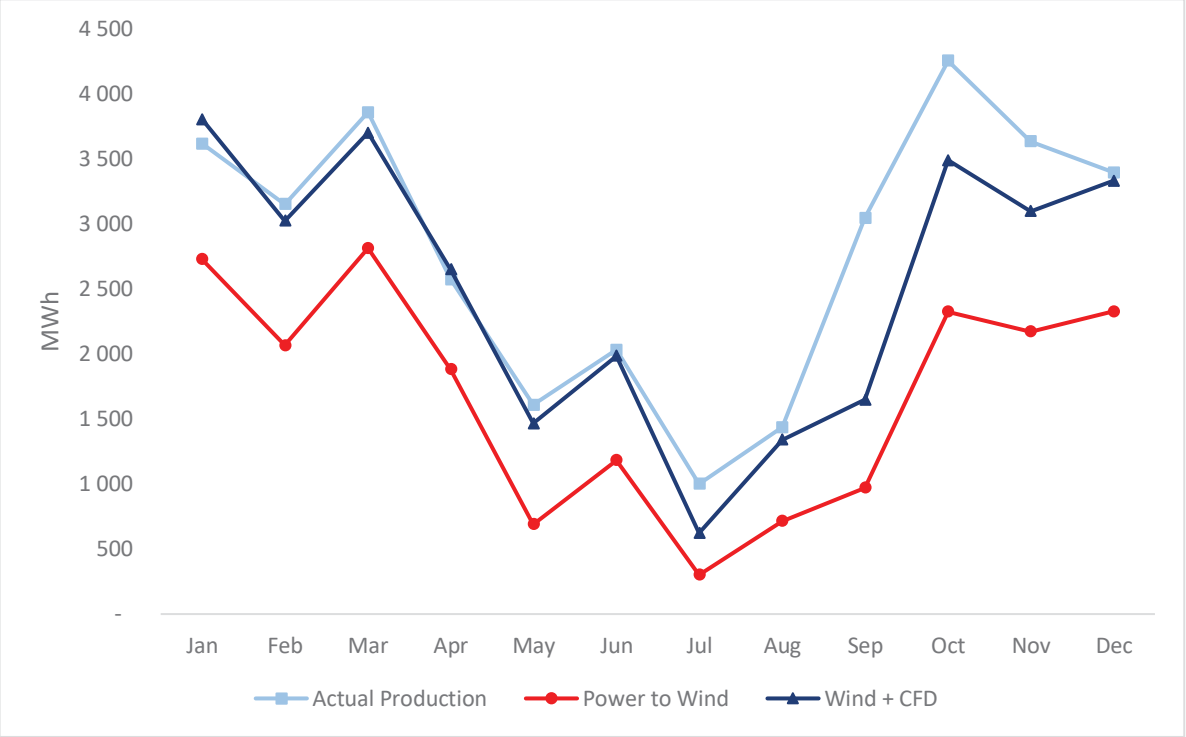

Figure 23 – Production forecast Valsneset

The historical data provided by NVE give a total production of 33,591.90 MWh for the forecasting period. The results show that both strategies underestimate the total production. Strategy – *Wind to Power* underestimate the AEP with 13,421.78 MWh and Strategy – *Wind + CFD to Power* with 3443.99 MWh over the whole forecasting period.

4.4.2 Forecast Error

Measuring the performance of the two methods, *Wind to Power* have a NMAE of 17.80% and *Wind + CFD to Power* presents a NMAE of 15.58%. For Valsneset wind farm, the forecasting method which includes CFD presented a lower forecasting error compared to *Wind to Power* with 2.21%. Figure 24 visualises how the error measurement varies during the forecast period. Both strategies perform well until a shift in August where both methods underestimate the production.

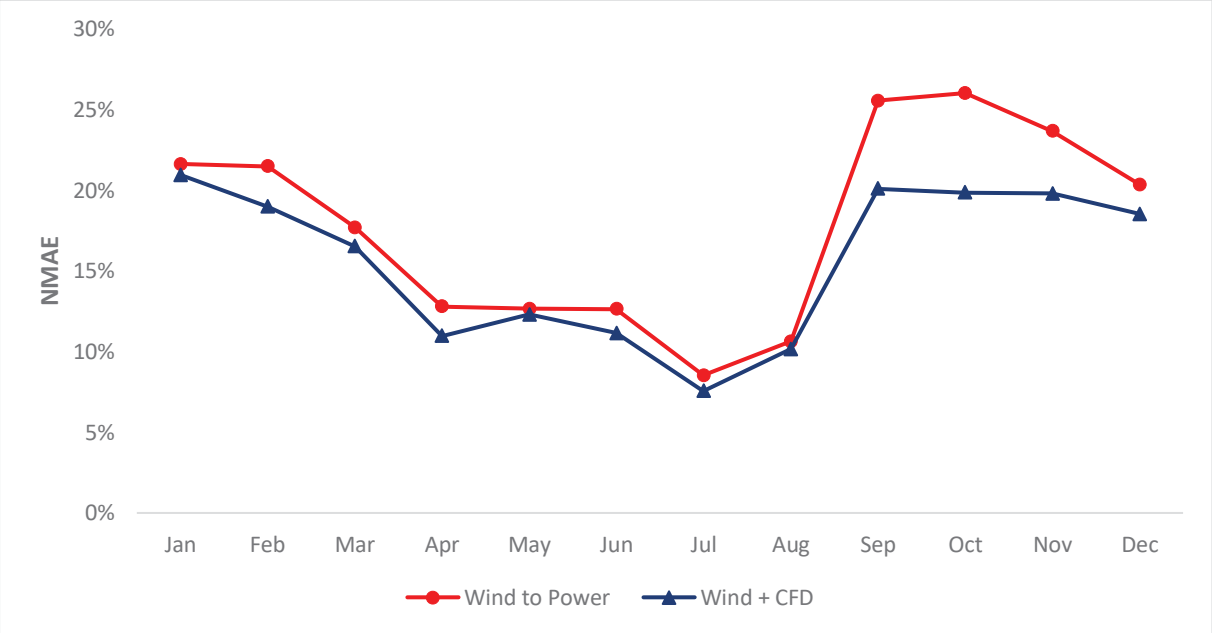

Figure 24 – Forecast error Valsneset

4.5 Ytre Vikna

4.5.1 Overall Production Forecast

For Ytre Vikna wind farm, forecasting strategy I – *Wind to Power* estimated a total production of 52,034.49 MWh. Strategy II – *Wind + CFD to Power* estimated it to be 144,826.22 MWh. The forecasted power predictions and the observed production is presented in Figure 25 on a monthly time-scale.

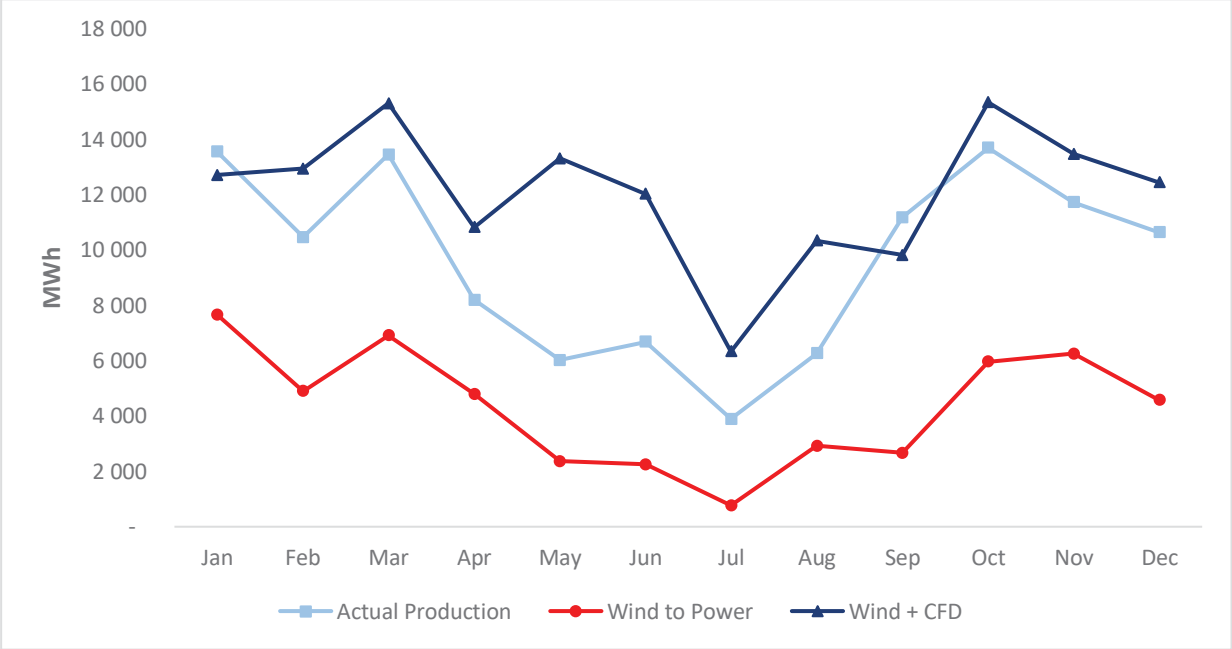

Figure 25 – Production forecast Ytre Vikna

The historical data provided by NVE give a total production of 115,748.54 MWh for the forecast period. The results show that method I underestimates the total production with 63,714.05 MWh, while method II overestimate the total production with 29,077.67 MWh over the total period.

4.5.2 Forecast Error

Measuring the performance of the two strategies, *Wind to Power* have a NMAE of 20.69% and *Wind + CFD to Power* presents a NMAE of 22.71%. For Ytre Vikna farm the forecasting strategy using the theoretical power curve produced the forecast with the lowest error measurement with a difference of difference 2.02%. Figure 26 visualises how the error measurement varies during the forecasting period. *Wind to Power* have a rapid change in error from August to September when the production increases in towards the winter months.

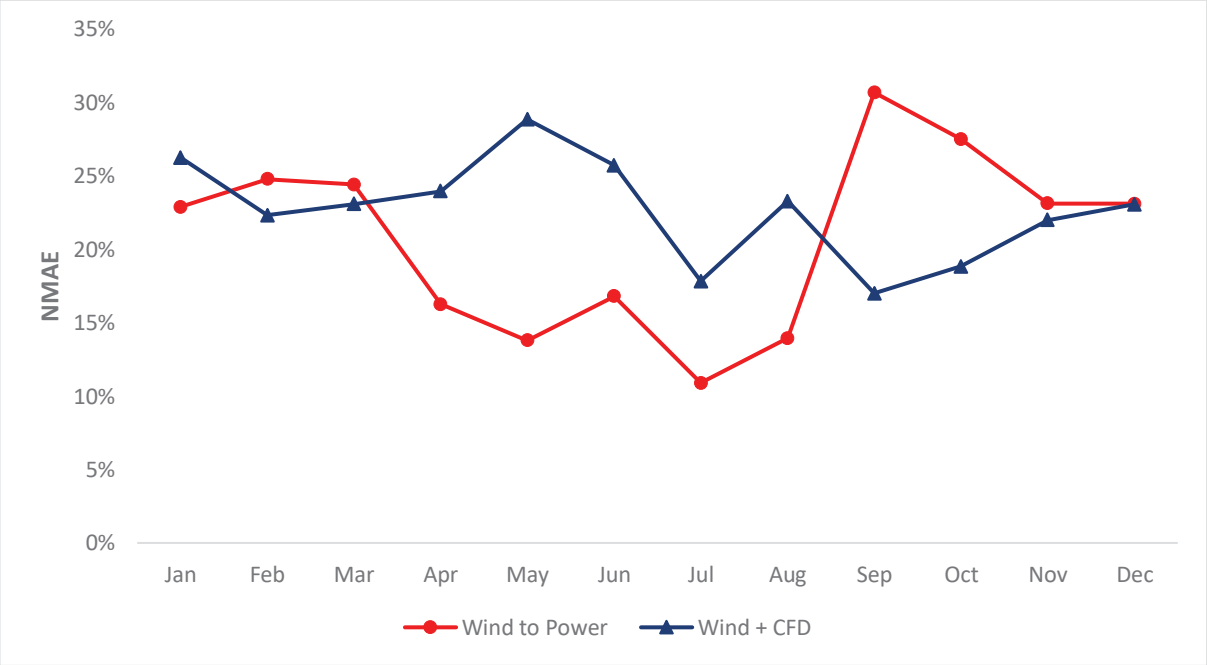

Figure 26 – Forecast error Ytre Vikna

4.6 Overall Results

The overall performance of the two forecast methods are presented in Table 5. In the case of Bessakerfjellet, Hitra and Valsneset wind farm, forecast strategy *Wind + CFD to Power* presented forecasts with 2. 63%, 4.42% and 2.21% lower NMAE compared to *Wind to power*. In the case of Smøla and Ytre Vikna, the *Wind to Power* strategy resulted in a NMAE which were 4.59% and 2.02% lower compered to *Wind + CFD to Power*. A summary of the overall results can be seen in Table 5.

Table 5 – Overall forecast error for 2017.

Wind Farm	Nominal Power (MW)	Wind to Power (NMAE)	Wind + CFD to Power (NMAE)	Difference
Bessakerfjellet	56.446	19.19%	16.56%	2.63%
Hitra	54.410	21.06%	16.64%	4.42%
Smøla	148.450	1321%	17.80%	-4.59%
Valsneset	11.710	17.80%	15.58%	2.21%
Ytre Vikna	38.800	20.69%	22.71%	-2.02%

4.7 Calibration Point Height Analysis

To investigate the effect of the selected height for the calibration point, three different production forecasts are estimated for Bessakerfjellet. This is done by setting the height (z-direction) of the calibration point to: 10m, 30m and 50m. The monthly NMAE is presented in Figure 27.

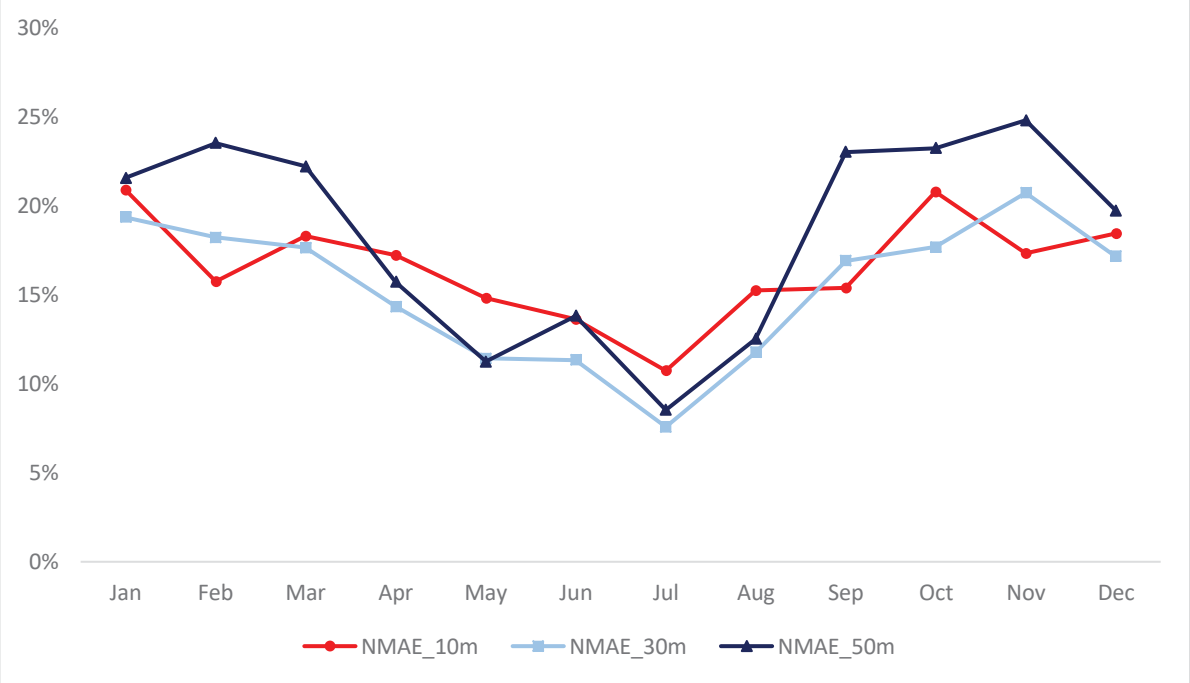

Figure 27 – Power + CFD to Wind Forecast Error at Bessakerfjellet

The total forecast error for the calibration point with height: 10m, 20m and 30m can be seen in Table 6. 10m was the original setting used when designing all the wind farms.

Table 6 – Calibration height analysis for Bessakerfjellet Wind Farm

NMAE Z-direction: 10m	NMAE Z-direction: 30m	NMAE Z-direction: 50m
16.56%	15.34%	18.30%

4.8 Periods of Interest

4.8.1 Production and Prediction Inconsistency

For the period of August 22 – 27 at Smøla Wind farm, Figure 28 exemplifies the inconsistency between the predicted power of the CFD method and the actual power prediction. The NMAE for this period is for the *Wind + CFD strategy* is 16.06% and for the *Wind to Power* it is 5.61%.

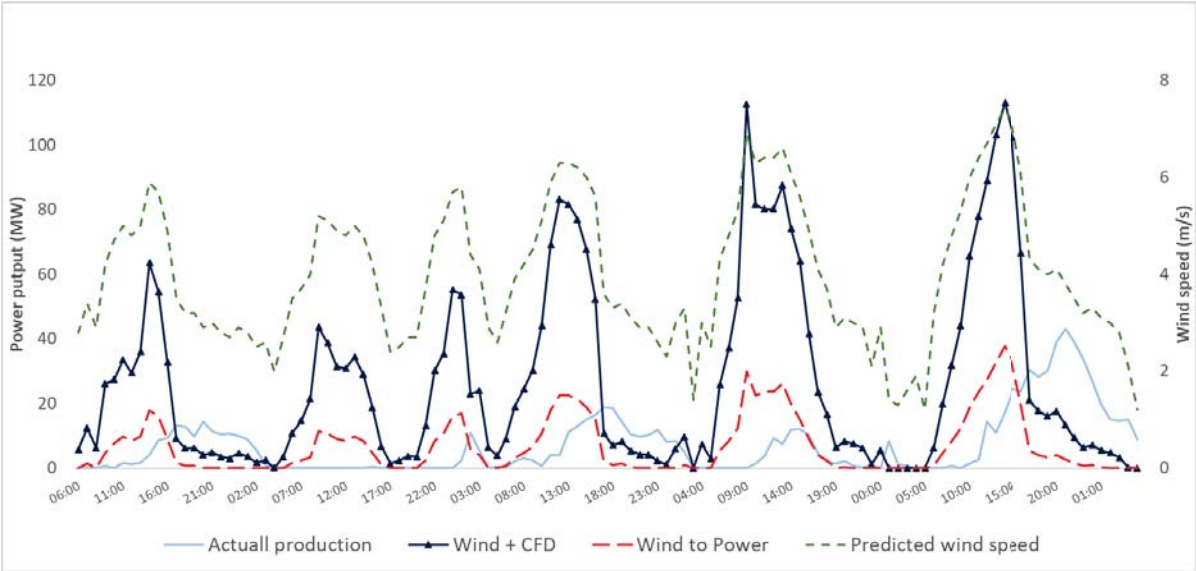

Figure 28 – Production and prediction inconsistency

4.8.2 Ramp Events

For the period of January 19 – 21 at Valsneset, a sudden change in the production occur. This event falls within the definition of a ramp event. The power output increased from approximately 0.8 MW to 11.3 MW in a period of less than 4 hours.

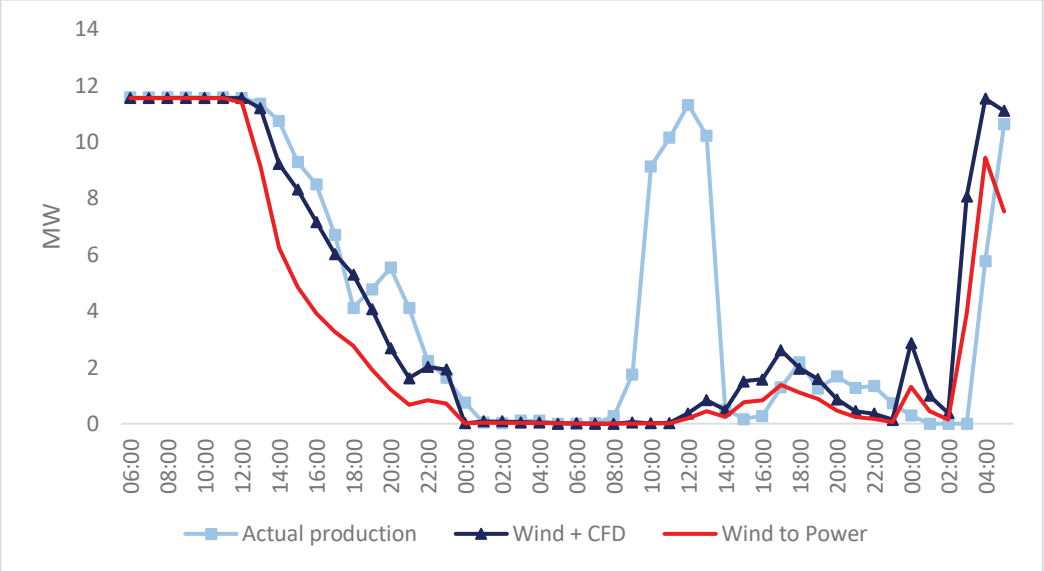

Figure 29 - Ramp event Valsneset

For the period of January 27 – 28 at Smøla, a sudden change in the production occur. This event falls within the definition of a ramp event. The power output increased from approximately 8 MW to 135 MW in a period of less than 4 hours.

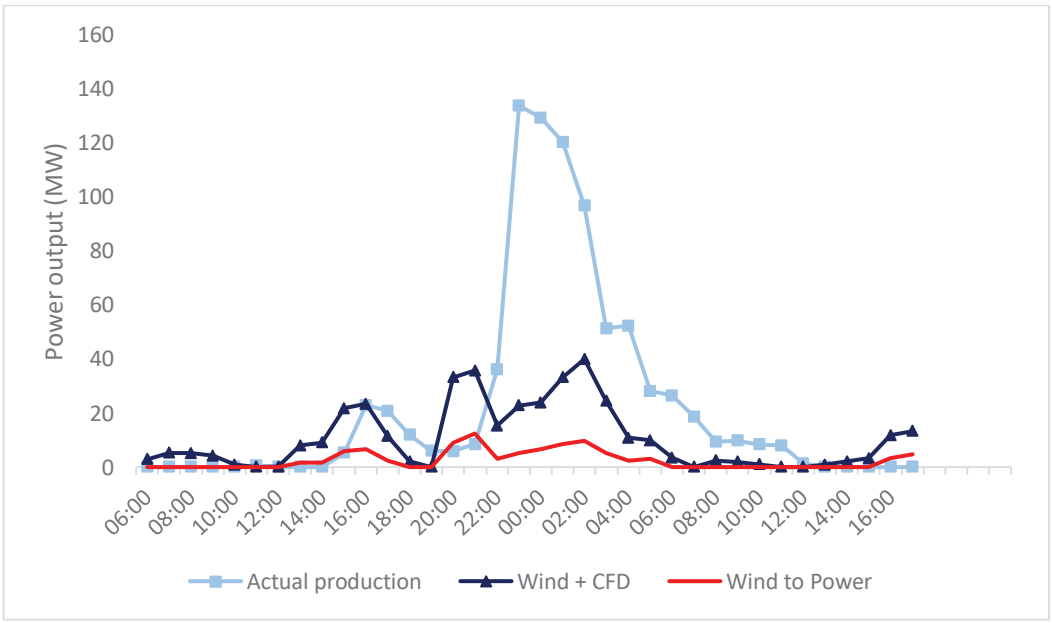

Figure 30 – Ramp event at Smøla

4.8.3 Period with High Accuracy

In the period of May 14 – 19 at Smøla wind farm there is a sudden change in the wind speed. As seen in Figure 31 an actual power output of 20 MW changes to 133 MW, the forecasted wind speed is highly accurate, and both strategies produce an accurate forecast. The NMAE for the Wind + CFD method is 12.85% and Wind to Power is 8.26%.

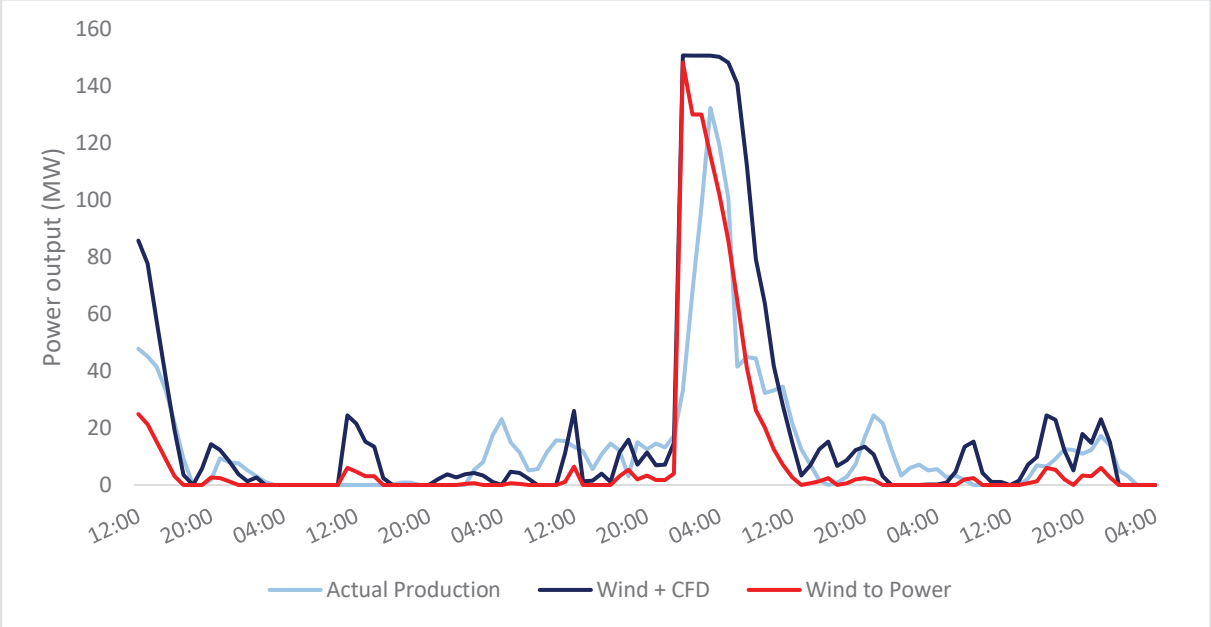

Figure 31 – Rapid change in wind speed at Smøla wind farm

5 Discussion

With the increased penetration of wind power in the energy system, accurate and reliable prediction models are regarded to be one of the central aspects to drive this development forward (Wang et al., 2011). Regarding accuracy and sources of error, the following section will discuss the subject.

5.1 The Data Foundation

The data foundation will always be of great influence on the results. For this project, the time series utilized have been based on forecasted wind speed time series and not actual measurements. Uncertainties and prediction errors in the forecasted wind speeds and directions would be adopted by the forecasting model. Because of this, an unknown part of the deviation could be traced back to the forecasted wind speeds provided by Yr.

To further increase the forecast performance, and improve the accuracy, the use of ANN could be beneficial. ANN has been applied in many studies and with promising results (Barbosa de Alencar et al., 2017). With the use of historical data, the neural network is trained, and in the process the neural network learns from its errors (Barbosa de Alencar et al., 2017). The results from the CFD method indicates that it could be systematic errors in the forecasts. Therefore, by correcting this systematic error, the accuracy could be improved.

5.1.1 Time Scales

There is a strong relationship between wind speed and the power output. The time resolution of the forecasted wind speeds and direction provided by Yr is based on hourly estimations. Because of this, potential variation between two time-steps are not accounted for in the time series. Wind speeds are stochastic of nature, and between two time-steps there could potentially be significant variation between the predicted wind speed and the actual wind occurring at the wind farm. If the forecasted wind speed diverges significantly from the actual wind speed, the forecasting model will not be able to account for the deviation.

The dataset provided by NVE is based on power production for the whole hour, and an eventual variety in the wind would result in changes in the power production, and therefore being observed.

5.2 Developing the WindSim Models

WindSim is an advanced simulation program, primarily used by experienced users. Prior to this project, a basic course and WindSim training were completed. Nevertheless, mastering a computational tool like WindSim requires practice and experience. Because of the time frame for this project, becoming a competent user is demanding. Therefore, some uncertainties related to the WindSim models could be caused by user error.

5.2.1 Grid Resolution and Computer Capacities

In terms of defining a maximum number of cells, the value of 500 000 cells were selected. The grid is defined and optimized within limitations of the upper limit. With an increase in the resolution of the model, it is plausible that the performance of the *Wind + CFD to Power* forecast could improve. Giebel et al. (2006) emphasized the importance of including an adequate number of vertical levels in the first 100m from ground level. This is also in compliance with the recommendations from Gravdahl and Meißner (2015). The wind farm models were within the recommended 6-8 cells in the first 100m, although a finer resolution would be desirable to better capture the terrain effects. The limitation of running more refined models is due to lack of computational capacities. The simulations have been run on a standard student laptop, and therefore limiting the possibilities of building a more refined model. In a project with a longer time frame and adequate computational capacities, a post-process analysis should be conducted. A grid sensitivity study for all the five wind farms are recommended. This could be done by improving the grid refinement and increasing the number of cells until the variation in estimated AEP is negligible, this could reduce the uncertainty related to the models (Gravdahl & Meißner, 2015).

5.2.2 Wake Modelling

Wakes in a wind farm is of great importance when analysing large wind farms. Especially if the placement of the turbines creates a row like pattern (Gravdahl & Meißner, 2015). To analyse the wakes effect, and to analyse the accuracy of the wake modelling, post-processing analysis could be conducted (Gravdahl & Meißner, 2015). In the case of Smøla, with a large number of turbines, the WindSim model designed could potentially underestimate the wake loss. Gravdahl and Meißner (2015) recommend calculating wake losses by applying linear sum and the sum of squares method and averaging those two results. This could have improved the accuracy and reduced the overestimated power output at Smøla.

5.2.3 Selected Height for the Calibration Point

The selected height of the calibration point has influence on how the WindSim model estimates the wind flow at turbine height. In the case where the calibration point is set too low, the model could potentially overestimate the production. This effect was seen when a calibration point analysis was conducted for Bessakerfjellet Wind Farm. With an increase to 30m, the NMAE was reduced to 15.34%, which is an improvement of 1.22%. By setting the calibration point to 50m, the NMAE increased with 1.74% compared to the default setting of 10m. The results indicate that there are some uncertainties connected to selected height of the calibration point. The results also indicate that the models overestimate the power output in the lower wind speed area (3-6m/s). Compared to the historical data, the CFD power predictions lies higher. It would therefore be beneficial to conduct a similar analysis for all the wind farms and remove eventual systematic error.

5.3 Theoretical Power Curve

The forecasting method *Wind to Power* is based on a theoretical power curve. The power output is derived as a function of the power curve and forecasted wind speeds. In terms of recreating the real conditions in the wind farm, the assumption of the theoretical method relies on uniform conditions. Sohoni et al. (2016) analysed wind turbine power curve modelling techniques and their applications in wind-based energy systems. They highlighted limitations with the use of a theoretical power curve. They found it not being able to account for the physical aspects (e.g. terrain roughness and orography). To obtain a more precise

representation of the turbines power output, an implementation of the actual condition at the wind farm would be preferable (Sohoni et al., 2016). This could have been done for forecasting method – *Wind to Power* the use of an empirical power curve could improve the accuracy.

5.4 Challenges with Forecasted Wind Speed

5.4.1 Ramp Events

The use of forecasted wind speeds in hourly time resolution impose some challenges. As seen in section 4.8.2 Ramp Events, the occurrence of sudden changes in wind speed can be hard to predict. The forecasted power output is therefore drastically underestimated, as seen in section 4.8.2 and Figure 29 and Figure 30. These extreme events do not occur with high frequency, but it should be of interest to monitor, as these drastic changes in production provides difficulties for the TSOs.

5.4.2 Timing

Regarding the timing of the wind speed, and when it is occurring at the wind farm, the results show some indications of deviation. This could be situations where the predicted wind speed misses the timing with plus/minus 5-6 hours for example. This is one of the challenges when using weather predictions. A large part of the production forecast relies on the quality of the weather forecast.

5.4.3 Production and Forecast Inconsistency

There are some examples of where the forecasted wind speeds do not occur, and the power historical power production is close to zero. The forecasting method which includes CFD will in these cases have a higher prediction error than the theoretical turbine method. It can be seen from Figure 28 how this reduces the total accuracy. It also occurs more often in for lower forecasted wind speeds (4-6 m/s).

6 Conclusion

6.1 Conclusion

For this project, one year of forecasted wind speed data from the weather service provider Yr has been used to predict the power output at five wind farms located in Norway. The first method is based on an equivalent power curve. The second method uses the computational fluid dynamics program WindSim to predict the power output. The results from the analysis found the forecasting method which uses CFD to produce the most accurate forecast in the case of Bessakerfjellet, Hitra and Valsneset, with a NMAE of 16.45%, 16.64% and 15.58% respectively. The forecasting method based on a theoretical turbine power curve performed best at Smøla and Ytre Vikna, with a NMAE of 13.21% and 20.69% respectively. The findings demonstrate the benefits of using CFD when prediction wind power production, and with additional adjustment of the prediction models, the accuracy could be further improved. The conclusion is to continue the work of implementing and developing the use of CFD in wind power forecasting.

6.2 Future Work

With the timeframe and size of this project, some aspects were excluded from the scope. Therefore, the following aspects are identified as interesting, and could be further investigated in future work.

- Include actual wind speed measurements. It would give insight to the relationship between the wind speed and power output at the wind farm locations.
- Historical power output data on per turbine level. It would give a more accurate foundation to benchmark the results against. It would also disclose potential periods with turbines unavailability e.g. maintenance periods and icing events or other forms of turbine unavailability.

7 References

Aarnes, J. F. & Aubert, K. E. (2018). *Interpolation - mathematics* Online Encylopedia Store norske leksikon Available at: https://snl.no/interpolasjon_-_matematikk (accessed: 04.05).

Anderson, J. D. & Wendt, J. (1995). *Computational Fluid Dynamics an Introduction* vol. 206: Springer.

Barbosa de Alencar, D., de Mattos Affonso, C., Limão de Oliveira, R., Moya Rodríguez, J., Leite, J. & Reston Filho, J. (2017). Different models for forecasting wind power generation: Case study. *Energies*, 10 (12): 1976.

Blazek, J. (2015). *Computational Fluid Dynamics: Principles and Applications*: Elsevier Science.

Castellani, F., Astolfi, D., Mana, M., Burlando, M., Meißner, C. & Piccioni, E. (2016). *Wind power forecasting techniques in complex terrain: ANN vs. ANN-CFD hybrid approach*. Journal of Physics: Conference Series: IOP Publishing.

Corbo, F., Mana, M. & Meißner, D. C. (2015). Benefits of using CFD for wind power forecasting in complex terrain *EWEA*.

DNV-GL. (2018). *Energy Transition Outlook 2018 - A global and regional forecast of the energy transition to 2050*. www.dnvgl.com.

Foley, A. M., Leahy, P. G., Marvuglia, A. & McKeogh, E. J. (2012). Current methods and advances in forecasting of wind power generation. *Renewable Energy*, 37 (1): 1-8.

Giebel, G., Badger, J., Perez, I. M., Louka, P., Kallos, G., Palomares, A., Lac, C. & Descombes, G. (2006). *Short-term forecasting using advanced physical modelling-the results of the anemos project*. Proceedings of the European Wind Energy Conference.

Gravdahl, A. & Meißner, C. (2015). *Best Practices - WindSim*. WindSim Basic Course. Unpublished manuscript.

Gravdahl, A. (2019). *WindSim Basic Course - Demo Project Hundhammerfjellet*. Gravdahl, A. (ed.): WindSim AS.

Greaves, B., Collins, J., Parkes, J. & Tindal, A. (2009). Temporal forecast uncertainty for ramp events. *Wind Engineering*, 33 (4): 309-319.

Hau, E. & Renouard, H. v. (2013). *Wind Turbines*. 3 ed. ed.: Germany: Springer Verlag.

Hervik, S. (2017). *Numerisk metode* Store Norske Leksikon www.snl.no.

Hiester, T. & Pennell, W. (1981). *Meteorological aspects of siting large wind turbines*: Battelle Pacific Northwest Labs., Richland, WA (USA).

Hoel, A. (2004). *A wind Bonus for Siemens*. POWER ENGINEERING INTERNATIONAL: POWER ENGINEERING INTERNATIONAL. Available at: https://www.powerengineeringint.com/articles/print/volume-12/issue-11/regulars/news-analysis/a-wind-bonus-for-siemens.html (accessed: 28.04).

Jensen Støver, I. (2019). *Om Yr* web page In Jensen Støver, I. (ed.). www.yr.no: NRK Available at: https://hjelp.yr.no/hc/no/articles/206550539-Fakta-om-Yr (accessed: 12.03).

Kariniotakis, G., Pinson, P., Siebert, N., Giebel, G. & Barthelmie, R. (2004). *The state of the art in short-term prediction of wind power-from an offshore perspective*. Proceedings of.

Landberg, L. & Watson, S. J. (1994). Short-term prediction of local wind conditions. *Boundary-Layer Meteorology*, 70 (1-2): 171-195.

Lei, M., Shiyan, L., Chuanwen, J., Hongling, L. & Yan, Z. (2009). A review on the forecasting of wind speed and generated power. *Renewable and Sustainable Energy Reviews*, 13 (4): 915-920.

Li, L., Liu, Y.-q., Yang, Y.-p., Shuang, H. & Wang, Y.-m. (2013). A physical approach of the short-term wind power prediction based on CFD pre-calculated flow fields. *Journal of Hydrodynamics, Ser. B*, 25 (1): 56-61.

Lont, A. (2018). *Annual report 2018* Statnett Annual Report 2018. https://www.statnett.no/en/about-statnett/investor-relations/annual-and-semi-annual-reports/.

Manwell, J. F., McGowan, J. G. & Rogers, A. L. (2010). *Wind Energy Explained: Theory, Design and Application*: Wiley.

Milligan, M., Schwartz, M. & Wan, Y.-h. (2003). *Statistical wind power forecasting models: Results for US wind farms*: National Renewable Energy Lab.(NREL), Golden, CO (United States).

NVE Atlas. (2019). *NVE atlas* NVE.no: The Norwegian Water Resources and Energy Directorate. Available at: https://atlas.nve.no/Html5Viewer/index.html?viewer=nveatlas# (accessed: 02.05).

Rosvold, K. & Hofstad, K. (2013). *Betz` Lov* Store Norske Leksikon. www.snl.no Store Norske Leksikon

Sohoni, V., Gupta, S. & Nema, R. (2016). A critical review on wind turbine power curve modelling techniques and their applications in wind based energy systems. *Journal of Energy*, 2016.

Soman, S. S., Zareipour, H., Malik, O. & Mandal, P. (2010). *A review of wind power and wind speed forecasting methods with different time horizons*. North American Power Symposium 2010: IEEE.

Søviknes, T. (2018). *Wind power in Norway post 2020*. Energy, M. o. P. a. Norwegian Govurnment: Berthelsen, Ole.

US Department of Energy. (2018). *The Inside of a Wind Turbine* US Department of Energy US Department of Energy. Available at: https://www.energy.gov/eere/wind/inside-wind-turbine (accessed: 22.03.).

Versteeg, H. K. & Malalasekera, W. (2007). *An Introduction to Computational Fluid Dynamics: The Finite Volume Method*: Pearson Education Limited.

Wang, X., Guo, P. & Huang, X. (2011). A review of wind power forecasting models. *Energy procedia*, 12: 770-778.

Wegley, H. L., Ramsdell, J. V., Orgill, M. M. & Drake, R. L. (1980). *Siting handbook for small wind energy conversion systems*: Battelle Pacific Northwest Labs., Richland, WA (USA).

Weir, D. E. (2013). NVE Vindkraft—Produksjon i 2012. *Norges Vassdrags-og Energidirektorat: Oslo, Norway*.

Willmott, C. J. & Matsuura, K. (2005). Advantages of the mean absolute error (MAE) over the root mean square error (RMSE) in assessing average model performance. *Climate research*, 30 (1): 79-82.

Wu, Y.-K. & Hong, J.-S. (2007). *A literature review of wind forecasting technology in the world*. 2007 IEEE Lausanne Power Tech: IEEE.

Zhao, X., Wang, S. & Li, T. (2011). Review of evaluation criteria and main methods of wind power forecasting. *Energy Procedia*, 12: 761-769.

8 Appendix A – Wind Turbine Effect Curves

Wind-speed (m/s)	Enercon E70 2.3MW (kW)	Bonus 2.0MW (kW)	Bonus 2.3MW (kW)
1	0	0	0
2	2	0	0
3	16	0	0
4	53	45	52
5	121	129	148
6	230	250	288
7	383	414	476
8	596	634	729
9	866	917	1055
10	1212	1234	1419
11	1580	1538	1769
12	1885	1775	2041
13	2077	1911	2198
14	2262	1971	2267
15	2300	1992	2291
16	2310	1998	2298
17	2310	2000	2300
18	2310	2000	2300
19	2310	2000	2300
20	2310	2000	2300
21	2310	2000	2300
22	2310	2000	2300
23	2310	2000	2300
24	2310	2000	2300
25	2310	2000	2300

Power Curve	Thrust coefficient
Enercon E-70 2.3 MW	
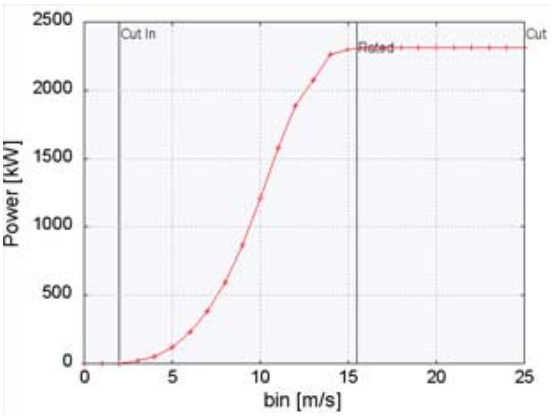	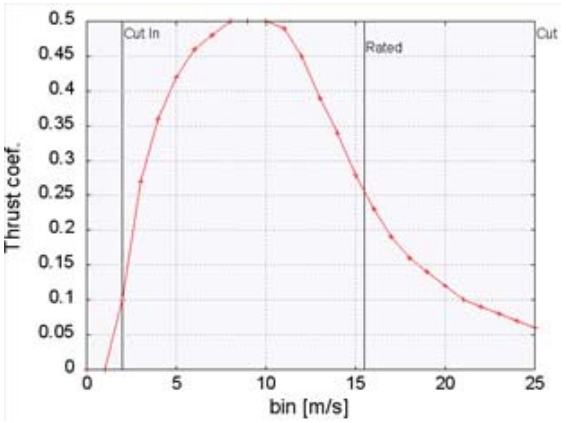
Bonus 2.0 MW 76*	
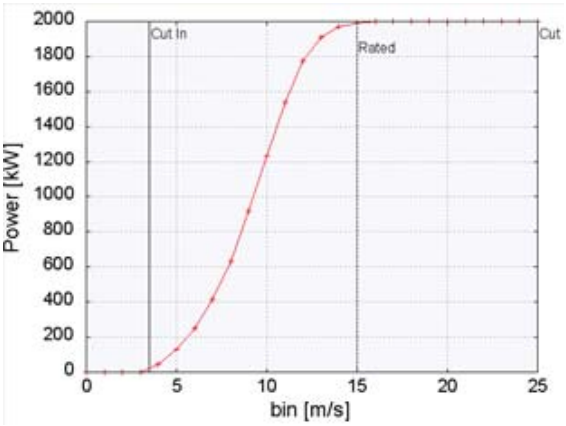	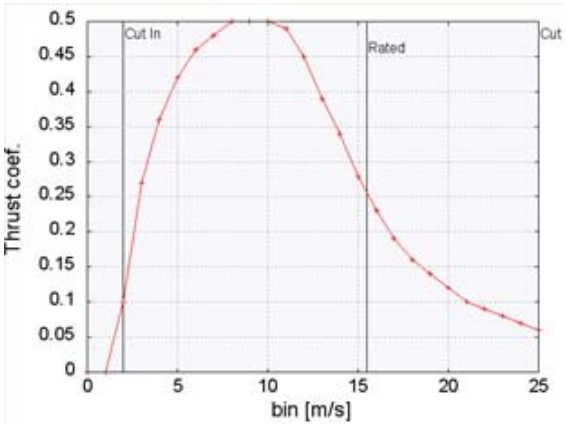
Bonus 2.3 MW 81	
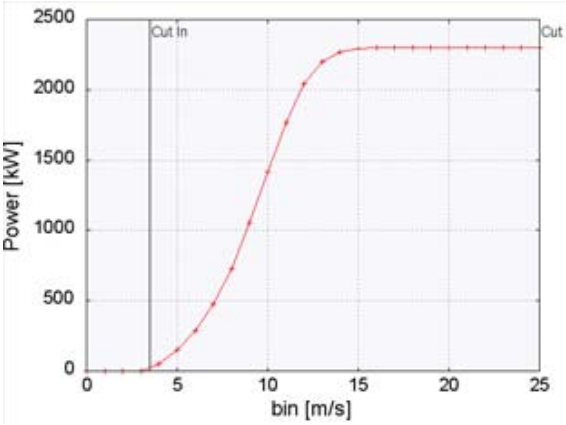	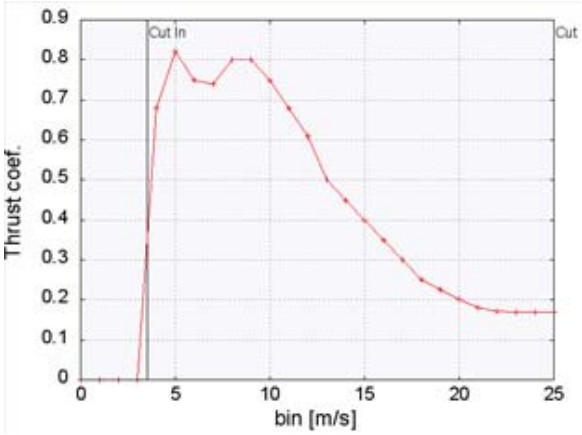

The effect curves are based on the wind turbine library found in simulation software WindPRO. These curves are published in the 2012 – Annual Wind report by NWE (Weir, 2013).

*The Bonus 2.0 MW effect curve is based on a down-scaled Bonus 2.3 MW turbine.

9 Appendix B – WindSim Report

Appendix B will present the outputs from the WindSim generated report, presenting the chosen standards for each of the five wind farms that have been analysed.

Hitra Wind Farm

Wind Farm Layout:

The wind farm consists of 24 turbines, with the technical specifications given in the following table.

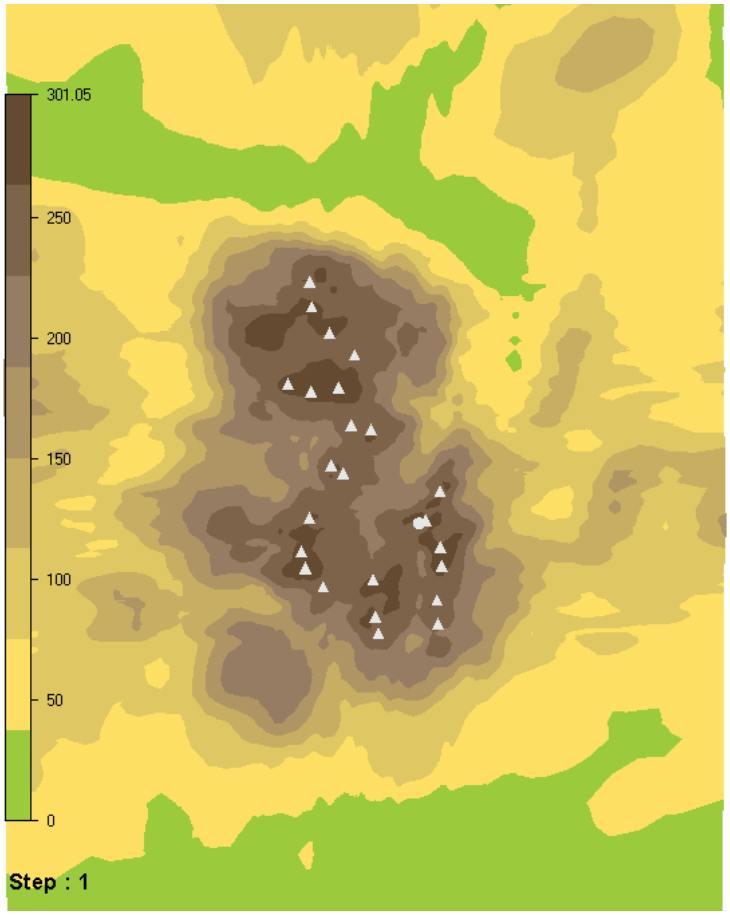

Wind farm layout; triangles represent turbines, dots represent climatology's

Turbine type	Rated wind speed (m/s)	Cut-in wind speed (m/s)	Cut-off wind speed (m/s)	Diameter (m)	air density (kg/m3)
2.3 MW	15	3	25	71.00	1.225

Numerical Simulations:

A numerical wind database is established by CFD simulations. The numerical wind database is used to transfer the wind conditions from the measurement point to the wind turbine hub positions. This chapter describes how the numerical model is set up, simulated and validated.

Digital Terrain Model:

The coordinate system is UTM, Zone: 32, Datum: WGS84, which is the coordinate system referred to whenever coordinates are used in this report. Note that the underlying datasets for elevation and roughness might have different resolution. The following online sources have been used for elevation: ASTER GDEM v2 Worldwide Elevation Data (1 arc-second Resolution) and for roughness: CORINE Land Cover Europe 2006 (100 m Resolution)

	Min (m)	Max (m)	Extension (m)	Resolution Terrain Data (m)
Easting (m)	484459.1	494462.9	10003.8	34.0
Northing (m)	7038007.0	7050603.0	12596.0	34.0

Coordinates, extensions and resolution of the digital terrain model referring to coordinate system: UTM, *Zone:* 32, *Datum:* WGS84

3D Model Setup:

The elevation and roughness data defined above is used to define the ground level of a three-dimensional domain divided in cells with a variable horizontal and vertical resolution. The grid is generated and optimized from the digital terrain model, as seen in the figure below.

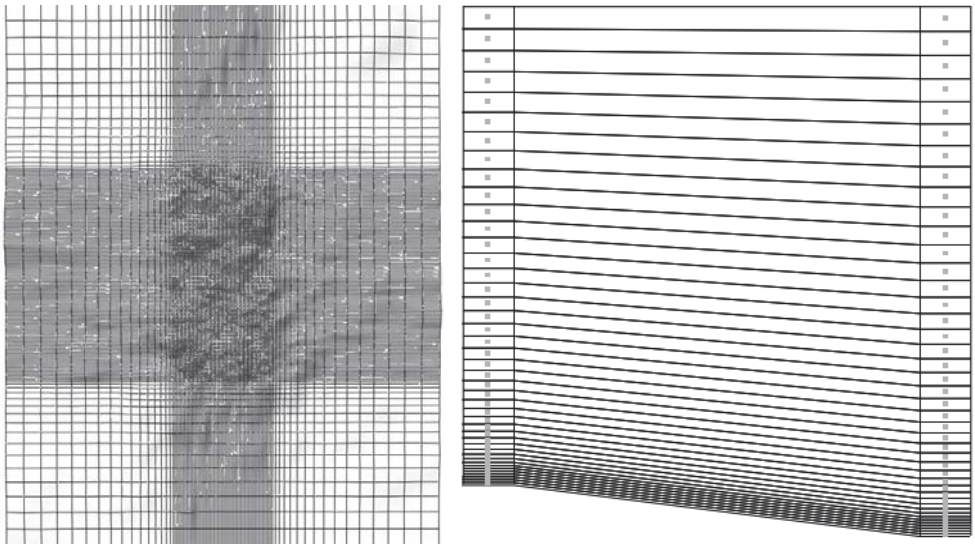

Horizontal grid resolution (left) and schematic view of the vertical grid resolution (right

	Easting	Northing	z	Total
Grid spacing (m)	45.0-413.8	45.2-413.6	Variable	-
Number of cells	83	140	43	499660

Grid spacing and number of cells

The grid extends 2854 (m) above the point in the terrain with the highest elevation. The grid is refined towards the ground. The left and right columns display a schematic view of the distribution at the position with maximum and minimum elevation respectively. The nodes, where results from the simulations are available, are situated in the cell centres indicated by dots.

	1	2	3	4	5	6	7	8	9	10
z-dist. max (m)	8.3	25.0	41.7	58.3	75.0	91.7	108.3	126.4	147.8	172.3
z-dist. min (m)	8.3	25.0	41.7	58.3	75.0	91.7	109.2	129.3	153.1	180.4

Distribution of the first 10 nodes in z-direction, relative to the ground, at the position with maximum and minimum elevation

Simulations:

The digital model represents the computational domain where the Reynolds averaged Navier – Stokes equations have been numerically solved. In total 36 simulations have been performed to have a 3D wind field for every 10-degree sector.

Height of boundary layer (m)	500.0
Speed above boundary layer (m/s)	10.0
Boundary condition at the top	fix pres.
Potential temperature	No
Turbulence model	Standard
Solver	GCV
Maximum iterations	500
Convergence criteria	0,001

Solver settings

Bessakerfjellet Wind Farm

Wind Farm Layout:

The wind farm consists of 25 turbines, with the technical specifications given in the following table.

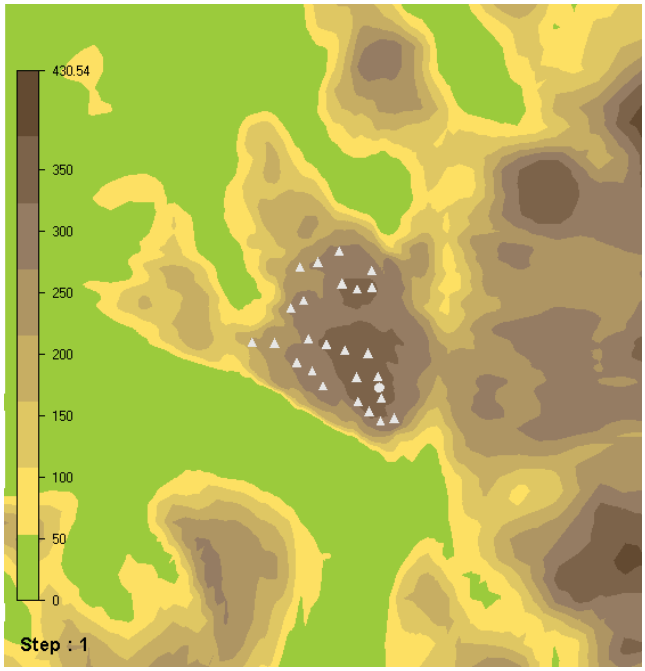

Wind farm layout; triangles represent turbines, dots represent climatology's

Turbine type	Rated wind speed (m/s)	Cut-in wind speed (m/s)	Cut-off wind speed (m/s)	Diameter (m)	air density (kg/m3)
2.3MW	15	2	25	71.00	1.225

Numerical Simulations:

A numerical wind database is established by CFD simulations. The numerical wind database is used to transfer the wind conditions from the measurement point to the wind turbine hub positions. This chapter describes how the numerical model is set up, simulated and validated.

Digital Terrain Model:

The coordinate system is UTM, Zone: 32, Datum: WGS84, which is the coordinate system referred to whenever coordinates are used in this report. Note that the underlying datasets for elevation and roughness might have different resolution. The following online sources have been used for elevation: ASTER GDEM v2 Worldwide Elevation Data (1 arc-second Resolution) and for roughness: CORINE Land Cover Europe 2006 (100 m Resolution).

	Min (m)	Max (m)	Extension (m)	Resolution Terrain Data (m)
Easting (m)	561258.5	571268.3	10009.8	34.0
Northing (m)	7117477.0	7127892.0	10415.0	34.0

Coordinates, extensions and resolution of the digital terrain model referring to coordinate system: UTM, *Zone:* 32, *Datum:* WGS84

3D Model Setup:

The elevation and roughness data defined above is used to define the ground level of a three-dimensional domain divided in cells with a variable horizontal and vertical resolution. The grid is generated and optimized from the digital terrain model, as seen in the figure below.

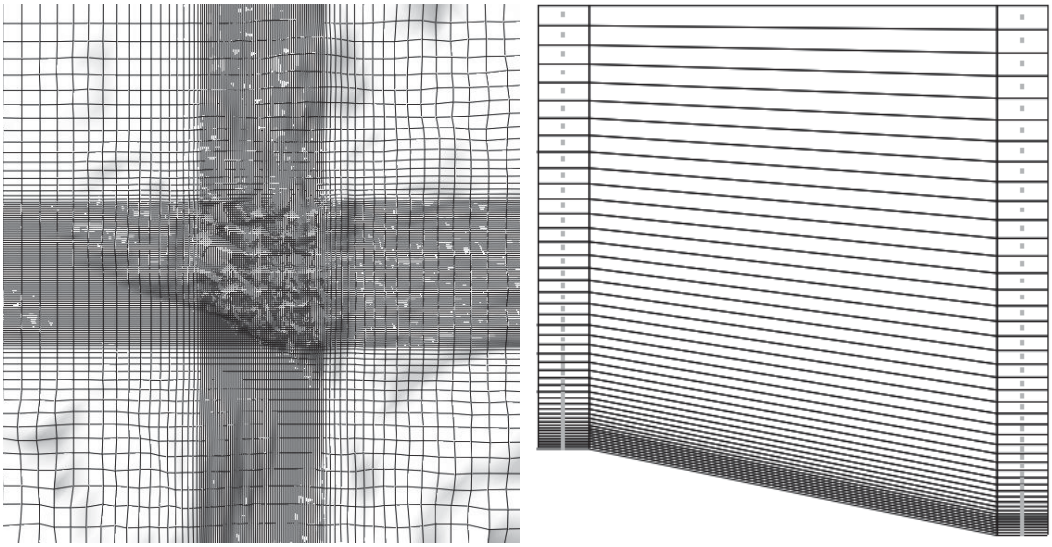

Horizontal grid resolution (left) and schematic view of the vertical grid resolution (right)

	Easting	Northing	z	Total
Grid spacing (m)	36.3-370.1	36.9-392.1	Variable	-
Number of cells	101	110	45	499950

Grid spacing and number of cells

The grid extends 2423 (m) above the point in the terrain with the highest elevation. The grid is refined towards the ground. The left and right columns display a schematic view of the distribution at the position with maximum and minimum elevation respectively. The nodes, where results from the simulations are available, are situated in the cell centres indicated by dots.

	1	2	3	4	5	6	7	8	9	10
z-dist. max (m)	7.1	21.4	35.7	50.0	64.3	78.6	92.9	106.6	121.2	138.4
z-dist. min (m)	7.1	21.4	35.7	50.0	64.3	78.6	92.9	108.0	125.5	146.2

Distribution of the first 10 nodes in z-direction, relative to the ground, at the position with maximum and minimum elevation

Simulations:

The digital model represents the computational domain where the Reynolds averaged Navier – Stokes equations have been numerically solved. In total 36 simulations have been performed to have a 3D wind field for every 10-degree sector.

Height of boundary layer (m)	500.0
Speed above boundary layer (m/s)	10.0
Boundary condition at the top	fix pres.
Potential temperature	No
Turbulence model	Standard
Solver	GCV
Maximum iterations	500
Convergence criteria	0,001

Solver settings

Smøla Wind Farm

Wind Farm Layout:

The wind farm consists of 68 turbines, with the technical specifications given in the following table. The wind farm is built in two steps. The first step includes 20. 2.0 MW Turbines, and step two consists of 48 2.3 MW turbines.

Turbine type	Rated wind speed (m/s)	Cut-in wind speed (m/s)	Cut-off wind speed (m/s)	Diameter (m)	air density (kg/m3)
2.0MW	15	3	25	76.00	1.225
2.3MW	15	2	25	71.00	1.225

Numerical Simulations:

A numerical wind database is established by CFD simulations. The numerical wind database is used to transfer the wind conditions from the measurement point to the wind turbine hub positions. This chapter describes how the numerical model is set up, simulated and validated.

Digital Terrain Model:

The coordinate system is UTM, Zone: 32, Datum: WGS84, which is the coordinate system referred to whenever coordinates are used in this report. Note that the underlying datasets for elevation and roughness might have different resolution. The following online sources have been used for elevation: ASTER GDEM v2 Worldwide Elevation Data (1 arc-second Resolution) and for roughness: CORINE Land Cover Europe 2006 (100 m Resolution).

	Min (m)	Max (m)	Extension (m)	Resolution Terrain Data (m)
Easting (m)	439303.7	452540.2	13236.5	34.1
Northing (m)	7024249.0	7037747.0	13498.0	34.1

Coordinates, extensions and resolution of the digital terrain model referring to coordinate system: UTM, *Zone:* 32, *Datum:* WGS84

3D Model Setup:

The elevation and roughness data defined above is used to define the ground level of a three-dimensional domain divided in cells with a variable horizontal and vertical resolution. The grid is generated and optimized from the digital terrain model, as seen in the figure below.

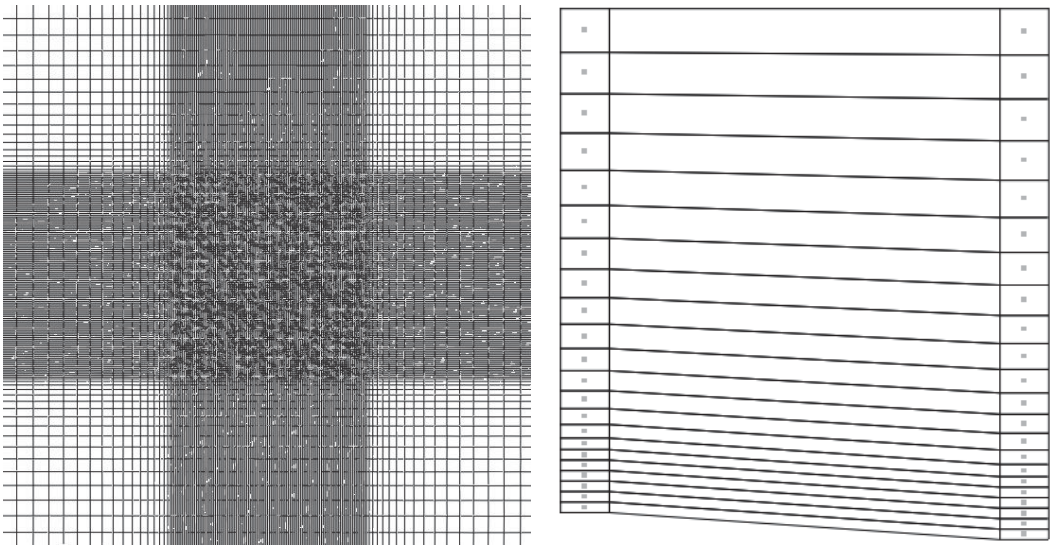

Horizontal grid resolution (left) and schematic view of the vertical grid resolution (right)

	Easting	Northing	z	Total
Grid spacing (m)	42.6-429.7	42.3-430.0	Variable	-
Number of cells	147	154	22	498036

Grid spacing and number of cells

The grid extends 813 (m) above the point in the terrain with the highest elevation. The grid is refined towards the ground. The left and right columns display a schematic view of the distribution at the position with maximum and minimum elevation respectively. The nodes, where results from the simulations are available, are situated in the cell centres indicated by dots.

	1	2	3	4	5	6	7	8	9	10
z-dist. max (m)	8.3	25.0	41.7	58.3	75.0	91.7	109.1	129.0	152.4	179.1
z-dist. min (m)	8.3	25.0	41.7	58.3	75.0	91.7	109.7	130.8	155.6	184.0

Distribution of the first 10 nodes in z-direction, relative to the ground, at the position with maximum and minimum elevation

Simulations:

The digital model represents the computational domain where the Reynolds averaged Navier – Stokes equations have been numerically solved. In total 36 simulations have been performed to have a 3D wind field for every 10-degree sector.

Height of boundary layer (m)	500.0
Speed above boundary layer (m/s)	10.0
Boundary condition at the top	fix pres.
Potential temperature	No
Turbulence model	Standard
Solver	GCV
Maximum iterations	500
Convergence criteria	0,001

Solver settings

Valsnset Wind Farm

Wind Farm Layout:

The wind farm consists of 5 turbines, with the technical specifications given in the following table.

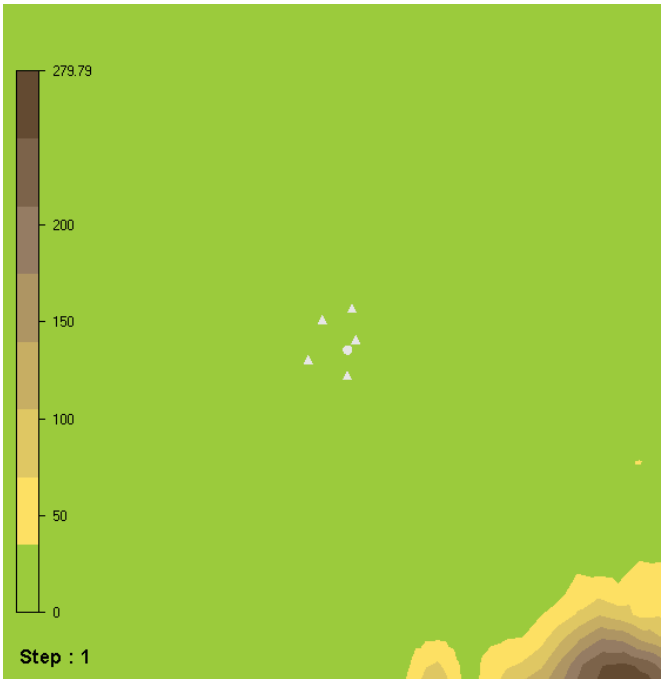

Wind farm layout; triangles represent turbines, dots represent climatology's

Turbine type	Rated wind speed (m/s)	Cut-in wind speed (m/s)	Cut-off wind speed (m/s)	Diameter (m)	air density (kg/m3)
2.3MW	15	2	25	71.00	1.225

Numerical Simulations:

A numerical wind database is established by CFD simulations. The numerical wind database is used to transfer the wind conditions from the measurement point to the wind turbine hub positions. This chapter describes how the numerical model is set up, simulated and validated.

Digital Terrain Model:

The coordinate system is UTM, Zone: 32, Datum: WGS84, which is the coordinate system referred to whenever coordinates are used in this report. Note that the underlying datasets for elevation and roughness might have different resolution. The following online sources

have been used for elevation: ASTER GDEM v2 Worldwide Elevation Data (1 arc-second Resolution) and for roughness: CORINE Land Cover Europe 2006 (100 m Resolution).

	Min (m)	Max (m)	Extension (m)	Resolution Terrain Data (m)
Easting (m)	527830.3	533931.2	6100.9	34.1
Northing (m)	7074016.0	7080286.0	6270.0	34.1

Coordinates, extensions and resolution of the digital terrain model referring to coordinate system: UTM, *Zone:* 32, *Datum:* WGS84

3D Model Setup:

The elevation and roughness data defined above is used to define the ground level of a three-dimensional domain divided in cells with a variable horizontal and vertical resolution. The grid is generated and optimized from the digital terrain model, as seen in the figure below.

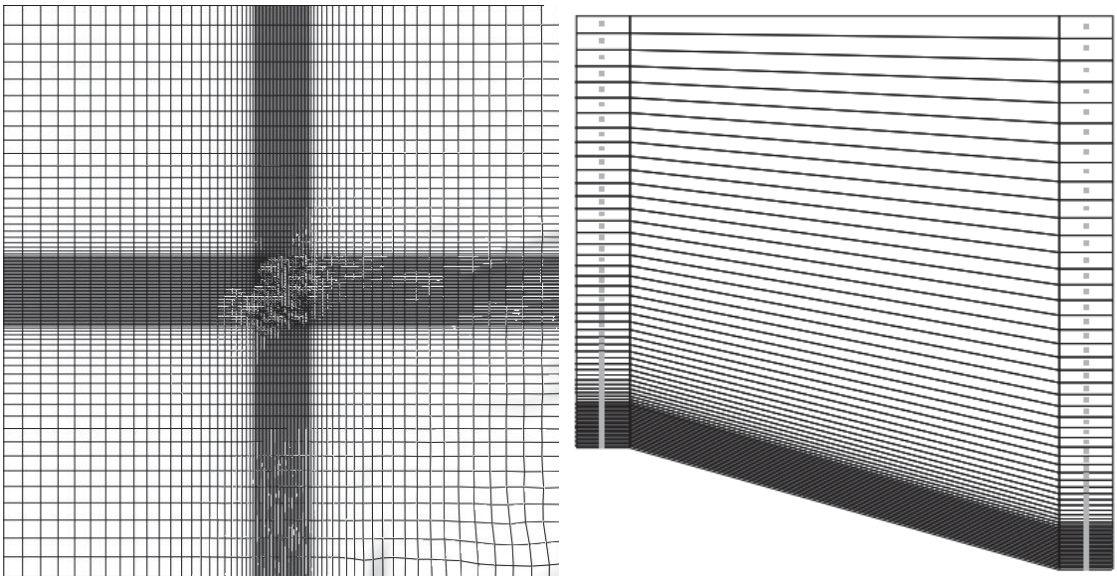

Horizontal grid resolution (left) and schematic view of the vertical grid resolution (right)

	Easting	Northing	z	Total
Grid spacing (m)	15.2-206.3	15.6-215.2	Variable	-
Number of cells	87	95	60	495900

Grid spacing and number of cells

The grid extends 1039 (m) above the point in the terrain with the highest elevation. The grid is refined towards the ground. The left and right columns display a schematic view of the distribution at the position with maximum and minimum elevation respectively. The nodes, where results from the simulations are available, are situated in the cell centres indicated by dots.

	1	2	3	4	5	6	7	8	9	10
z-dist. max (m)	2.6	7.9	13.2	18.4	23.7	28.9	34.2	39.5	44.7	50.0
z-dist. min (m)	2.6	7.9	13.2	18.4	23.7	28.9	34.2	39.5	44.7	50.0

Distribution of the first 10 nodes in z-direction, relative to the ground, at the position with maximum and minimum elevation

Simulations:

The digital model represents the computational domain where the Reynolds averaged Navier – Stokes equations have been numerically solved. In total 36 simulations have been performed to have a 3D wind field for every 10-degree sector.

Height of boundary layer (m)	500.0
Speed above boundary layer (m/s)	10.0
Boundary condition at the top	fix pres.
Potential temperature	No
Turbulence model	Standard
Solver	GCV
Maximum iterations	500
Convergence criteria	0,001

Solver settings

Ytre Vikna Wind Farm

Wind Farm Layout:

The wind farm consists of 5 turbines, with the technical specifications given in the following table.

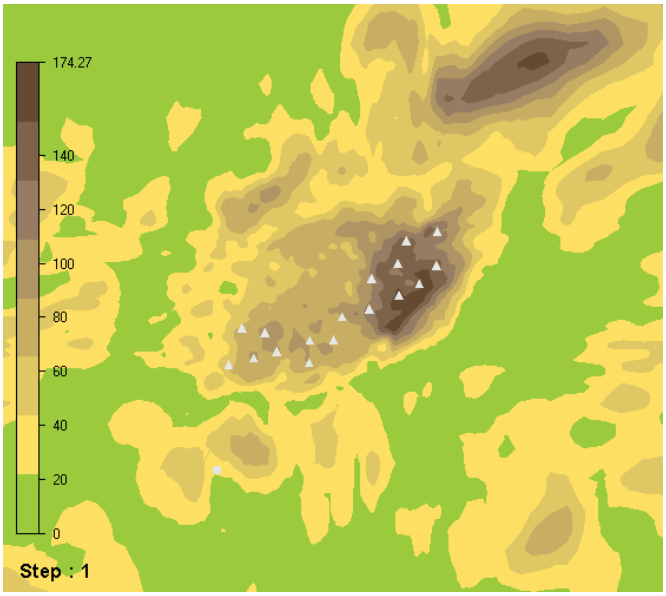

Wind farm layout; triangles represent turbines, dots represent climatology's

Turbine type	Rated wind speed (m/s)	Cut-in wind speed (m/s)	Cut-off wind speed (m/s)	Diameter (m)	air density (kg/m3)
2.3MW	15	2	25	71.00	1.225

Numerical Simulations:

A numerical wind database is established by CFD simulations. The numerical wind database is used to transfer the wind conditions from the measurement point to the wind turbine hub positions. This chapter describes how the numerical model is set up, simulated and validated.

Digital Terrain Model:

The coordinate system is UTM, Zone: 32, Datum: WGS84, which is the coordinate system referred to whenever coordinates are used in this report. Note that the underlying datasets for elevation and roughness might have different resolution. The following online sources have been used for elevation: ASTER GDEM v2 Worldwide Elevation Data (1 arc-second Resolution) and for roughness: CORINE Land Cover Europe 2006 (100 m Resolution).

	Min (m)	Max (m)	Extension (m)	Resolution Terrain Data (m)
Easting (m)	585481.0	593570.0	8089.0	32.1
Northing (m)	7195597.0	7202819.0	7222.0	32.0

Coordinates, extensions and resolution of the digital terrain model referring to coordinate system: UTM, *Zone:* 32, *Datum:* WGS84

3D Model Setup:

The elevation and roughness data defined above is used to define the ground level of a three-dimensional domain divided in cells with a variable horizontal and vertical resolution. The grid is generated and optimized from the digital terrain model, as seen in the figure below.

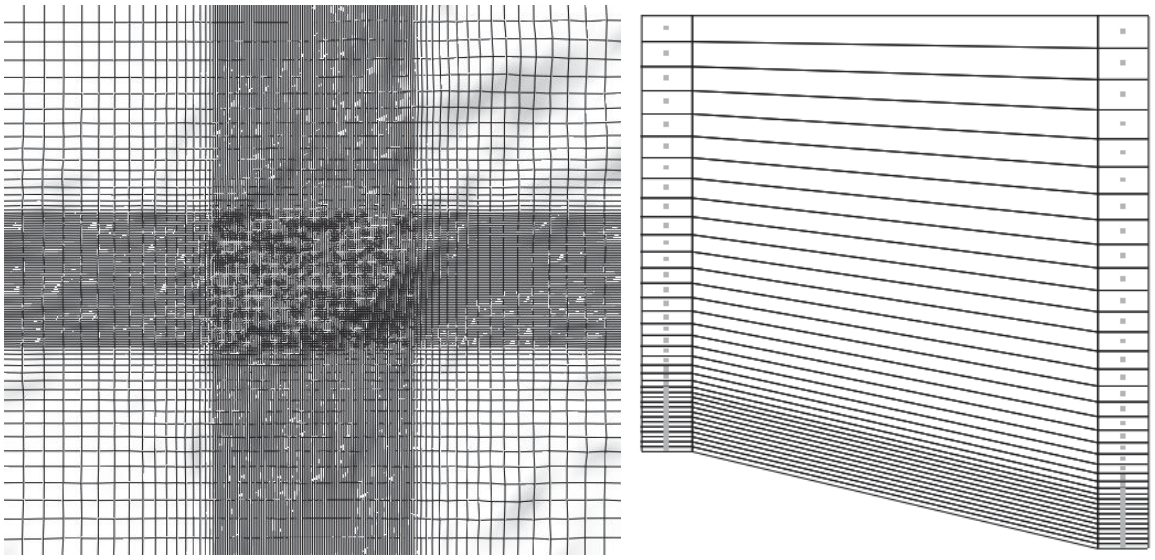

Horizontal grid resolution (left) and schematic view of the vertical grid resolution (right)

	Easting	Northing	z	Total
Grid spacing (m)	26.3-281.4	25.9-265.6	Variable	-
Number of cells	134	103	36	496872

Grid spacing and number of cells

The grid extends 804 (m) above the point in the terrain with the highest elevation. The grid is refined towards the ground. The left and right columns display a schematic view of the distribution at the position with maximum and minimum elevation respectively. The nodes, where results from the simulations are available, are situated in the cell centres indicated by dots.

	1	2	3	4	5	6	7	8	9	10
z-dist. max (m)	4.5	13.6	22.7	31.8	40.9	50.0	59.1	68.2	77.3	86.4
z-dist. min (m)	4.5	13.6	22.7	31.8	40.9	50.0	59.1	68.2	77.3	86.4

Distribution of the first 10 nodes in z-direction, relative to the ground, at the position with maximum and minimum elevation.

Simulations:

The digital model represents the computational domain where the Reynolds averaged Navier – Stokes equations have been numerically solved. In total 36 simulations have been performed to have a 3D wind field for every 10-degree sector.

Height of boundary layer (m)	500.0
Speed above boundary layer (m/s)	10.0
Boundary condition at the top	fix pres.
Potential temperature	No
Turbulence model	Standard
Solver	GCV
Maximum iterations	500
Convergence criteria	0,001

Solver settings

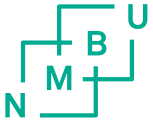

Norges miljø- og biovitenskapelige universitet
Noregs miljø- og biovitskapelege universitet
Norwegian University of Life Sciences

Postboks 5003
NO-1432 Ås
Norway